Cortical Functional Connectivity in Mouse Models of Early Blindness: Enucleation vs. Anophthalmia

G. Laliberté and D. Boire

Département d'anatomie, Université du Québec à Trois-Rivières, Trois-Rivières, Québec, Canada G9A 5H7

Corresponding author: Denis Boire, denis.boire@uqtr.ca

Running title: Functional Connectivity in Blind Mouse Models

Abstract

Early sensory deprivation drives large-scale reconfiguration of cortical networks, yet we still lack a clear understanding of the relative contributions of early visual experience versus spontaneous prenatal retinal waves on the establishment of the cortical network. We compared two mouse models of congenital blindness: neonatal enucleation and congenital anophthalmia, across two genetic strains (C57Bl/6J and ZRDBA) using mesoscopic calcium imaging of spontaneous activity and graph-theoretical analysis. Spectral analyses revealed localized strain-specific increases in infraslow and low delta power following visual deprivation, with C57Bl/6J enucleated and ZRDBA anophthalmic mice exhibiting more generalize nodal increase. Concomitantly, network organization was redirected toward medial higher-order visual areas, the associative retrosplenial cortex, and somatosensory regions, while the primary and lateral visual cortices exhibited reduced influence and integration within the modular architecture. Notably, ZRDBA groups

showed limited global changes to their cortical network. However, anophthalmic ZRDBA mice, lacking prenatal retinal waves, exhibited connectivity patterns more akin to enucleated C57Bl/6J than to their enucleated littermates, highlighting the instructive role of spontaneous prenatal retinal activity. These findings support a connectivity-constrained, experience-dependent model in which preexisting structural pathways guide diffuse, resilient reorganization following sensory loss.

Keywords: Resting-state functional connectivity, Cross-modal plasticity, early visual deprivation, Neonatal enucleation, Anophthalmia

Introduction

Individuals with visual impairments often display increased sensitivity to intact sensory modalities such as touch (Sadato *et al.* 1996; Goldreich and Kanics 2006; Ptito *et al.* 2012), auditions (Lessard *et al.* 1998; Roder *et al.* 1999; Collignon *et al.* 2006; Poirier *et al.* 2006; Bedny *et al.* 2011), and olfaction (Renier *et al.* 2013) (see López-Bendito *et al.* 2022 for review). These hypersensitivities to the intact sensory modalities in early blind patients coincide with the crossmodal activation of visual cortical areas (Bedny *et al.* 2011; Ptito *et al.* 2012; Renier *et al.* 2013; van der Heijden *et al.* 2019). Moreover, the functional significance of these crossmodal activations is demonstrated as transcranial magnetic inactivation of these visual areas reduce the crossmodal discriminative capabilities in early blind individuals (Amedi *et al.* 2004; Collignon *et al.* 2009).

This phenomenon reflects experience-dependent reconfiguration of brain connectivity. In early blind individuals, resting-state functional connectivity (rsFC) between primary visual cortex (V1) and primary sensory or motor cortices is diminished, while connectivity with frontoparietal cognitive networks is enhanced (Yu *et al.* 2008; Burton *et al.* 2014; Heine *et al.* 2015; Bauer *et al.* 2017; Abboud and Cohen 2019). These changes suggest a functional redirection of V1 away from sensory integration towards alternative pathways of higher-order processing (Liu *et al.* 2007; Bedny *et al.* 2011; Watkins *et al.* 2012; Burton *et al.* 2014; Wang *et al.* 2014; Striem-Amit *et al.* 2015; Kanjlia *et al.* 2016).

Interestingly, similar patterns are observed in sighted newborns who lack visual experience, suggesting that long-range cortical connectivity is initially sculpted by intrinsic mechanisms and later refined through sensory input (Tian *et al.* 2023). In contrast to blind

adults, sighted adults display stronger functional connectivity between V1 and non-visual sensory cortices, pointing to a dual influence of development and sensory experience in shaping cortical architecture (Tian *et al.* 2023).

Within this framework, the connectivity-constrained experience dependency hypothesis (see Saccone *et al.* 2024), suggests that preexisting structural connectivity constrains how cortical areas can be repurposed following sensory deprivation. This theoretical framework predicts that when ascending thalamocortical information is absent during development, as in congenital blindness, the predominance of descending pathways, such as the influence of the associative cortex, will prevail in conveying information to the deprived cortical areas (Murphy *et al.* 2016).

Unlike primates, rodents possess smaller, more fully interconnected cortices, with a reduced hierarchical structure (Harris *et al.* 2019) and direct interconnectivity between modality specific sensory areas even at the early stages of processing (Meredith and Lomber 2017; Gamanut *et al.* 2018; Gamanut and Shimaoka 2022; Magrou *et al.* 2024). In mice, visual cortices receive important descending inputs and display bidirectional connectivity with associative cortices, suggesting their potential multisensory or integrative roles even in sighted conditions (Charbonneau *et al.* 2012; Harris and Mrsic-Flogel 2013; Harris and Shepherd 2015; Petrus *et al.* 2015; Gamanut *et al.* 2018).

Interestingly, dorsal and ventral visual streams have been recognized in rodents (Wang *et al.* 2012; Harris *et al.* 2019; D'Souza *et al.* 2022) which bear notable functional similarities with their primate counterparts (Andermann *et al.* 2011; Glickfeld *et al.* 2013; Glickfeld and Olsen 2017; Saleem 2020). However, these pathways are more tightly interconnected

than in primates, consistent with the more shallow cortical hierarchy, the less modular, and more integrated cortical architecture observed in rodents (Oh *et al.* 2014; Zingg *et al.* 2014; Andelin *et al.* 2018; Gamanut *et al.* 2018; Gamanut and Shimaoka 2022; Magrou *et al.* 2024).

In mice, visual cortices are also taken over by the remaining sensory modalities following early blindness (Bonaventure and Karli 1968; Piché *et al.* 2004; Chabot *et al.* 2007; Iurilli *et al.* 2012; Petrus *et al.* 2014; Oude Lohuis *et al.* 2024). However, given their dense, non-hierarchical connectivity, it could be expected that rodents exhibit milder changes in functional connectivity between sensory-motor areas and between dorsal and ventral visual streams than those reported in primates. The shallow cortical hierarchy and high interconnectivity (Gamanut and Shimaoka 2022) make the mouse brain a valuable model for investigating how early visual deprivation reshapes neural networks, potentially supporting more distributed and resilient reorganization than in the modular primate cortex.

Ultimately, these interspecies differences raise a central question: Does early blindness lead to distinct modes of cortical reorganization depending on species-specific network architecture? The intrinsic interconnectivity of the rodent brain may favor more diffuse and flexible reorganization compared to the more modular and hierarchically structured cortex of primates.

In this context, we used two models of early blindness, neonatal enucleation and congenital anophthalmia, to explore how the timing and presence of early retinal activity shape cortical connectivity. While both models disrupt vision during critical developmental windows (Hensch 2005; López-Bendito *et al.* 2022), they differ in the preserved early spontaneous retinal activity in the enucleated mice.

The maturation of retinothalamic pathways is initially driven by spontaneous retinal waves (Meister *et al.* 1991; Wong *et al.* 1993; Blankenship and Feller 2010; Ackman *et al.* 2012) which propagate to the thalamus (Mooney *et al.* 1996; Weliky and Katz 1999) and reach the cortex (Dupont *et al.* 2006; Hanganu *et al.* 2006; Colonnese 2014). Prenatal retinal (Cang *et al.* 2005) and thalamic activity (Anton-Bolanos *et al.* 2019) are critical for proper cortical maps formation. Since thalamocortical projections reach the cortical plate around birth in mice (Miller *et al.* 1993), spontaneous retinal activity can still contribute to early visual structuring in neonatally enucleated mice. In contrast, anophthalmic mice in which the eyecup does not form (Chase and Chase 1941) receive no spontaneous retinal activity, leading to altered thalamocortical and intracortical connectivity during development (Godement *et al.* 1979; Rhoades *et al.* 1984, 1985; see also Olavarria *et al.* 1988; Laramée *et al.* 2014).

While crossmodal plasticity is well documented across species, the developmental mechanisms driving these changes remain poorly characterized. In particular, the respective contributions of prenatal and early postnatal input to the establishment of long-range cortical wiring are not yet well defined. This study seeks to address these gaps by employing mesoscopic calcium imaging of spontaneous activity in two complementary mouse models of early blindness: neonatal enucleation and congenital anophthalmia. By directly comparing these conditions, we aim to disentangle the influence of spontaneous prenatal sensory-driven activity from that of early postnatal deprivation. Together, these insights highlight the need for controlled experimental models to parse how timing and sensory experience interact with intrinsic network architecture to shape cortical

reorganization. In doing so, our work offers new perspectives on connectivity-constrained, experience-dependent plasticity.

Material and Methods

Mice

The Animal Care Committee of the University of Quebec at Trois-Rivières (CBSA, protocol DB17) approved all procedures, which adhered to the guidelines of the Canadian Council on Animal Care.

Two mouse strains were used in this study, C57Bl/6J and ZRDBA mice from our animal facility. The ZRDBA mouse line (Touj *et al.* 2019), derived from crossing sighted DBA-6 with the anophthalmic ZRDCT mice (Chase and Chase 1941) which features a key genetic mutation at the *ey1* locus on chromosome 18, crucial for developing structures like the retina (Tucker *et al.* 2001). Offspring from this cross can either be sighted or anophthalmic, depending on the genetic inheritance of the mutation, allowing for a direct comparison of anophtalmia and early enucleation within a single strain and even littermates. Twenty-two mice were used in this analysis, distributed into five experimental groups based on strain and eye status. These groups included C57Bl/6J sighted (n=5) and enucleated (n=3) mice, as well as ZRDBA sighted (n=5), enucleated (n=4), and anophthalmic (n=5) mice.

All mice were weaned at 3 weeks, and, except for neonatal enucleation, experimental procedures begins when they reached 6 weeks of age. Data acquisition was conducted between 3 and 6 months of age. Mice were housed in a room with a 12-hour light cycle and provided *ad libitum* access to food and water.

Enucleation

Upon observing the pup's birth, the dams received a dose of long-action Buprenorphine SR-LAB (1,0 mg/kg, Chiron Compounding Pharmacy Inc., Guelph, ON). Within 24 hours following birth, bilateral enucleation of half the sighted pups was performed under deep hypothermia induced anesthesia. The palpebral fissure was slit open with a scalpel and the eyeball was gently extracted, sectioning the optic nerve. The ocular orbits were filled with Gelfoam (Spongostan, Johnson & Johnson, New Brunswick, NJ, USA) and the eyelids were sealed with tissue adhesive (Vetbond, 3M, St. Paul, MN, USA). Afterward, the pups were warmed until fully awake and returned to their home cage.

Intravenous Viral Vector Injection

To target neuronal populations for calcium imaging, viral vectors with the AAV2/PHP.eB capsids were employed to deliver plasmids expressing the GCaMP6s calcium reporter, driven by the human synapsin promoter (AAV-hSyn-GCaMP6s; construct-889-aavphp-eb). The synapsin promoter is commonly used for a broad and stable neuron-specific expression in the cortex (Finneran *et al.* 2021) while minimizing expression in glial cells (Kugler *et al.* 2003; Jin *et al.* 2016). The viral vectors were injected into both C57Bl/6J and ZRDBA mice, aged 6-8 weeks. The viral vectors, provided by the Canadian Neurophotonics Platform Viral Vector Core Facility (RRID:SCR_016477), were delivered via the caudal vein, with a total volume of 300 µL of sterile phosphate-buffered saline (PBS) containing the viral suspension (6.0×10^{11} genome copies).

The PhP.eB serotype ability to cross the blood-brain barrier (Chan *et al.* 2017; Michelson *et al.* 2019) in both C57Bl/6J and DBA mice (Matsuzaki *et al.* 2019) allows for delivery into the bloodstream and an efficient neuronal transduction throughout the cortical mantel.

Implantation of the Chronic Imaging Chamber

At 8-10 weeks of age, all animals were administered a subcutaneous injection of Buprenorphine SR-LAB (1,0 mg/kg, Chiron Compounding Pharmacy Inc., Guelph, ON), anesthetized with isoflurane (induction at 5%, maintenance at 2% in medical O_2), and secured in a stereotaxic frame. Body temperature was maintained at 37°C using a heating pad and continuously monitored with a rectal thermometer. Additionally, when applicable, the eyes were shielded from corneal dehydration using lubricating veterinary ophthalmic gel (Aventix Pet Eye Lube, Aventix Animal Health, Burlington, ON, Canada).

The scalp was shaved and cleaned with chlorhexidine (2% v/v), ethanol (70% v/v), and iodine (16% v/v). Local anesthesia of the scalp was induced with a subcutaneous injection of mixture of Lidocaine 2% and Bupivacaine 0.25% (Lidocaine 7mg/kg, Bupivacaine 3.5mg/kg). The skin covering the skull was then replaced with transparent dental cement (C&B MetaBond, Parkell, Edgewood, NY, USA) with an overlying cover glass (Carolina, Burlington, NC, USA). A titanium bar (Labeo Technologies Inc.; 1.1 g, 25 x 3.2 x 3.2 mm; SKU: 515301) was added for head fixation during recording sessions.

Upon surgery completion, mice were given a subcutaneous injection of carprofen (0.5 mg/kg) and individually placed in clean cages for recovery. Subcutaneous injections of carprofen (0.5 mg/kg) were administered at 24-, 48-, and 72-hour post-surgery.

Following a recovery period of 5 days, females were grouped in sets of 3 to 5, while males were paired in cages, separated by clear plexiglass walls to facilitate social interaction while preventing aggression.

Mesoscale Calcium Imaging Recordings

To minimize potential circadian cycle-related biases, all data acquisition sessions were conducted within the same daily period (between 8 AM and 2 PM). To minimize stress,

mice were gradually habituated to head-fixation over a period of 5 days: initially for 5 minutes on the apparatus without head fixation, followed by increasing duration of the head fixation (5 minutes, 10 minutes, 20 minutes, and 40 minutes). For the first four days of habituation, brain illumination was off, while on the last day (during the 40-minute head-fixed session), brain illumination was activated. This process effectively reduced signs of stress both within the enclosure and during the experiment, as evidenced by sufficient grooming behaviour, reduced audible vocalization, decreased movements during the head fixation, and stable weight measurements.

During the experimental procedure, mice were head-fixed in darkness under the wide-field calcium imaging system (Labeo Technologies Inc.; OiS200). Calcium-sensitive signals were captured using a vertically positioned CCD camera (NIKKOR 50mm f/1.2, Nikon, Minato, Tokyo, Japan). For the application of hemocorrection, brain illumination was achieved through a sequence of 472 nm, 590 nm, and 623 nm light emissions. GCaMP6s calcium indicators were excited using 472 nm blue light (Cree XLamp XP-E2 LEDs, Cree, Durham, NC, USA), while alterations in the absorption of 590 nm and 623 nm wavelengths (Amber LED, LZ4-00MA00, and Red LED, LZ4-00MA00, OSRAM, Markham, Ontario, Canada) respectively enabled extraction of hemodynamic intrinsic signals associated with oxy- and deoxyhemoglobin (Valley *et al.* 2020).

The imaging acquisition rate was 30 Hz (10 Hz per wavelength while hemocorrection was applied and 30 Hz of 472 nm light for the spectral analysis) with a resolution of 512 x 512 pixels. Illumination levels were adjusted to ensure accurate signal capture without under- or oversaturation. An exposure time of 14.33 ms was employed, and the inclusion of a

long-pass filter at 496 nm, aligned with the imaging objective, effectively mitigated contamination from other wavelengths.

Spectral analysis was conducted on a single 15-minute resting-state acquisition without hemodynamic correction. Otherwise, all other analyses were based on four hemocorrected resting-state acquisitions, each lasting 15 minutes, for a total of 1 hour of data per subject. All sessions were performed using wide-field calcium imaging in a dark and silent environment, spaced over a 4 to 6-week period.

Data Processing and Analysis of Calcium Signals

Data preprocessing was performed with the Universal Mesoscale Imaging Toolbox (UmIT Bipolar- v2.0.0; [an open-source project maintained by LabeoTech; available at labeotech.github.io/Umit]). Images were categorized by wavelength and spatially downsampled to 128x128 pixels (10.7 µm/pixel) using the *run_ImagesClassification* function.

Spectral Analysis

The preprocessing and analysis pipeline began by removing linear trends from the entire recording using the *apply_detrend* function. The data was then temporally filtered and normalized with a bandpass filter ranging from 0.01 to 12 Hz using the *normalizeLPF* function. This frequency range allows for the investigation of the power of four distinct neuronal oscillations intervals: infraslow (<0.1 Hz), delta (0.1 – 4 Hz), theta (4 – 7 Hz), and mu (7.5 – 12 Hz). To eliminate potential habituation effects and ensure a stable baseline, the first 120 seconds and last 60 seconds of the data were trimmed using *trim_movie*. Next, Gaussian spatial filtering (*spatialGaussFilt*, with a sigma of 2) was applied to reduce spatial noise. The Mouse Allen Brain Atlas top projection mask, which

represents cortical areas, was then overlaid onto the cortical surface using *ROImanager*. The cortical mask (Figure 1) was aligned with the estimated bregma position of the acquisition, and its size adjusted based on the pixel/mm ratio. The regions of interest (ROIs) representing all cortical areas were slightly reduced (trimmed by 5 pixels) to ensure exclusive sampling within each area.

The average time series from pixels in 20 cortical areas (AC, RS, TEA, M1, M2, HL, TR, FL, BC, NO, MO, S2, PM, AM, A, V1, RL, AL, LM, and AU) from the right hemisphere were then extracted and subjected to spectral analysis using the *pspectrum* function in MATLAB (version 2024.2, The MathWorks, Inc., Natick, Massachusetts, USA). Finally, differences between the blind and sighted experimental groups from similar mouse lines were compared in the power spectral analysis.

Network Analysis

Hemodynamic signal corrections followed the protocol of Valley *et al.* (2020), performed with the *run_HemoCorrection* function. After detrending (*apply_detrend*), global signal regression (*GSR*) was applied to remove non-neuronal oscillations, including cardiac and respiratory influences (Turley *et al.* 2017). For alignment, frames from each acquisition were registered to an initial reference frame, ensuring consistency across sessions (*alignFrames*), with accuracy validated by an experienced observer. Temporal band-pass filtering was then applied to isolate target frequency range, specifically 0.01–0.1 Hz for infraslow frequencies (*normalizeLPF*). A Gaussian spatial filter ($\sigma = 2$) was used for spatial noise reduction (*spatialGaussFilt*). Acquisitions were trimmed, omitting the initial 120 seconds and final 60 seconds as explained for the spectral analysis (*trim_movie*). Next, Pearson's correlations were computed between the average activity of each pixel within

the 20 cortical areas in both hemispheres. Correlation matrices were normalized using fisher Z transform (*genCorrelationMatrix*). We employed the z-score correlation matrix of resting-state functional connectivity, with thresholds ranging from 0.1 to 0.4 (in 0.05 increments), to generate adjacency matrices (illustrated in supplementary figure 1) and for subsequent graph analysis. Various graph metrics were calculated, including density (*density_und*), global efficiency (*efficiency_wei*), strengths (*strengths_und*), eigenvector centrality (*eigenvector_centrality_und*), community structure (*community_louvain*), participation coefficient (*participation_coef*), betweenness centrality (*betweenness_wei*), module degree z-score (*module_degree_zscore*) and normalized mutual information between community partitions (*partition_distance*), all utilizing the Brain Connectivity Toolbox (Rubinov and Sporns 2010). All graphs were generated using a custom MATLAB function developed in-house, apart from the histograms, which was created using GraphPad Prism (version 10.5.0, GraphPad Software, Boston, MA, USA).

Statistical Analysis

Data were analyzed using IBM SPSS Statistics (Version 29.0.2.0; IBM Corp., Armonk, NY, USA). First, we compared the distributions of the power spectrum profile and Pearson's correlation using the Mann-Whitney test for the comparison between sighted and enucleated C57Bl/6J mice, and the Kruskal-Wallis test for the comparison between sighted, enucleated, and anophthalmic ZRDBA mice.

Second, we employed graph analysis to examine the structural and functional organization of brain networks, utilizing undirected weighted graphs derived from neuroimaging data. Both global (as detailed in the Global Network Metrics results section) and nodal metrics (described in the Nodal Influences and Community Structure results sections) were

calculated to assess the overall network properties, as well as the influence and structural role of individual nodes within the cortical network.

Comparisons between sighted and blind groups were performed separately within each mouse strain using multivariate analysis of variance (MANOVA) with Pillai's trace, applied to each set of graph metrics (as further described in the following sections). For the global network metrics, when MANOVA revealed a significant effect of visual status, Bonferroni-corrected pairwise comparisons were conducted to identify the specific metrics significantly altered by early blindness.

For the nodal influence and community structure metrics, when MANOVA indicated a combined effect of visual status and cortical areas, additional MANOVA analyses were carried out to determine which cortical regions were significantly affected. To systematically classify highly structuring or highly influential nodes, a thresholding approach was applied across the six Graph metrics used, three related to nodal influence (efficiency, connections quality and eigenvector centrality) and three assessing structural integration (within module centrality, participation coefficient and betweenness centrality), whereby nodes exceeding the mean plus one standard deviation were categorized as key hubs within the network. Following this, Bonferroni-corrected pairwise comparisons were applied to identify the specific graph metrics altered in those cortical regions due to early blindness.

To assess strain-dependent differences, we compared sighted and enucleated mouse strains while excluding the anophthalmic ZRDBA mice. This approach allowed us to evaluate the differential impact of enucleation across genetically distinct strains, accounting for

variability in visual cortex plasticity. When a significant multivariate effect was detected, Bonferroni-corrected pairwise comparisons were applied to identify specific metric differences between the two mouse strains.

Results

Spectral analysis

We compared the global (Figure 2 column i) and area-specific (Figure 2 column ii and iii) power spectra of cortical activity between sighted and blind mice to assess global and area-specific activity modifications (Figure 2 column iv). We focused our analysis on low-frequency oscillations, including infraslow (<0.1 Hz), delta (0.1 – 4 Hz), theta (4 – 7 Hz), and mu (8 – 12 Hz), which correspond to distinct neuronal oscillations associated with different levels of cortical processing (Uhlhaas *et al.* 2008). These slow oscillations characterize global processing modes that engage large cortical areas (Knyazev 2007). These global patterns of brain activity facilitate integration across cortical regions by synchronizing distributed neural assemblies (Nunez 2000). Such synchronization occurs through cross-frequency phase coupling, coordinating neuronal processing across multiple frequency bands (Palva and Palva 2018). Moreover, anatomical hub regions play a crucial role in this integration and in driving the synchronization of functional modules (Schmidt *et al.* 2015). By comparing these spectral domains, we aimed to identify specific alterations in cortical dynamics related to visual experience and sensory deprivation.

Global Power Spectrum Alterations

The power spectral distribution of cortical spontaneous activity was comparable between sighted and enucleated mice, and it was predominantly concentrated in low frequencies

(0.01–4 Hz) across most cortical regions. A gradual decline in power was observed at higher frequencies, with peak power in the infraslow range (Figure 2A-C column i).

In sighted C57Bl/6J mice (Figure 2A-i), the power spectrum was dominated by infraslow (40.13 ± 3.82%) and delta (58.26 ± 3.71%) frequency bands, consistent with the slow decay kinetics of the GCaMP6s calcium indicator. Higher-frequency components, including theta (0.75 ± 0.08%) and mu (0.80 ± 0.19%) bands, contributed minimally to the overall signal. Neonatal enucleation significantly altered this spectral profile (Pillai's trace: $V = 0.955$, $F = 21.107$, $df = 4$, $p = 0.006$). In the enucleated mice power was increased in the infraslow (57.64 ± 5.40%, $p = 0.033$) and delta (42.06 ± 5.25%, $p = 0.006$) bands. No significant changes were observed in theta (0.18 ± 0.12%) or mu (0.11 ± 0.27%) frequencies.

In ZRDBA mice, sighted mice (Figure 2B-C column i) exhibited power distributions of infraslow (49.37 ± 2.99%), delta (49.26 ± 3.17%), theta (0.70 ± 0.17%), and mu (0.80 ± 0.17%). Enucleated mice (Figure 2B-i) showed slight variations: infraslow (45.12 ± 3.35%), delta (53.20 ± 3.55%), theta (0.57 ± 0.19%), and mu (1.02 ± 0.35%). Anophthalmic mice (Figure 2C-i) exhibited similar distributions: infraslow (45.07 ± 2.99%), delta (53.76 ± 3.17%), theta (0.41 ± 0.17%), and mu (0.71 ± 0.31%). Despite these slight proportional differences, visual deprivation did not significantly influence the power spectrum ($V = 0.762$, $F = 1.385$, $df = 8$, $p = 0.268$).

Regional Power Spectrum Alterations

Analysis of the power distribution for each cortical area (Figure 2 column ii to iv) for the full spectrum [0.01–12 Hz]), revealed the most pronounced differences induced by enucleation and anophthalmia and in both mouse strains in the low-frequency range (0.01–

4 Hz), encompassing infraslow and low delta frequencies. Blind mice exhibited slightly elevated power in the 8–12 Hz range compared to sighted mice, particularly in the ZRDBA mice, while theta activity (4–8 Hz) power was generally low and unaltered by blindness in all regions.

C57Bl/6J Enucleated Mice (Figure 2A-iv)

Mapping of power differences in the infraslow frequency range on the cortical mantel showed a substantial increased power in the associative areas (AC, RS and TEA), as well as increased power in motor (M1 and M2), specific somatosensory regions, such as dorsal column-related areas (HL, FL and TR) and S2 and medial visual areas (A, AM and PM), in the enucleated compared to the intact sighted C57Bl/6J mice. Conversely, a reduction in infraslow power was detected in lateral visual regions (AL and LM), the auditory area (AU), and the somatosensory area representing mouth (MO) and nose (NO).

ZRDBA Enucleated Mice (Figure 2B-iv)

Although the global cortical power spectrum was unchanged in blind ZRDBA mice, differences in power levels were observed within specific cortical areas. Areas showing power changes in the enucleated ZRDBA mice were different than those in the enucleated C57Bl/6J mice. In the enucleated ZRDBA mice, a slight decrease in infraslow power was detected in some associative area (AC) and increase in other (RS and TEA), dorsal column-related somatosensory areas (FL, HL and TR), and most visual areas (except AL and LM which is enhanced). In contrast, infraslow power was increased in auditory region (AU), trigeminal-related somatosensory areas (BC, MO and NO), and S2.

ZRDBA Anophtalmic Mice (Figure 2C - iv)

Compared to sighted ZRDBA mice, mild infralow power increases were detected in the associative areas (RS and TEA), somatosensory regions (all except for MO and NO) and all visual areas were observed in the anophthalmic mice. Infraslow frequency of other areas were barely unaltered, except for a slight decrease in the associative anterior cingulate area (AC).

Effect of Mouse Strain and Visual Deprivation on the Global Power Spectrum

Finally, a multivariate analysis comparing sighted and enucleated mice across both strains revealed a significant effect of visual status on the power spectrum ($V = 0.642$, $F = 4.938$, $df = 4$, $p = 0.016$). However, neither mouse strain nor the interaction between visual status and strain had a significant effect, suggesting that the influence of visual status on spectral features was consistent across both strains.

Implications for Cortical Integration and Cross-Modal Plasticity

In C57Bl/6J mice, enucleation significantly increased infraslow and delta power, particularly in associative, motor, somatosensory and medial visual areas, suggesting enhanced global integration and cross-modal plasticity. In contrast, ZRDBA enucleated mice showed no global spectral shifts but exhibited localized changes, with increased power in auditory and trigeminal-related regions and decreases in somatosensory and visual areas, indicating a region-specific adaptation.

Interestingly, the infraslow power pattern of the anophthalmic ZRDBA mice was more like the enucleated C57Bl/6J mice than to the enucleated ZRDBA mice. However, the distinction between infraslow power pattern of both early blind ZRDBA mice suggests that the lack of prenatal spontaneous retinal wave in play a significant role in the development

of cortical functional connectivity. Overall, the differential effect of enucleation in both mice strain underscore the role of genetic background in shaping cortical plasticity following sensory loss.

Functional Connectivity Alterations

We used resting-state spontaneous activity correlations between 20 dorsal cortical areas per hemisphere to generate z-score normalized inter- and intrahemispheric functional connectivity matrices for each experimental group (Supplemental figure 1).

Inter- and Intrahemispheric Correlation Distribution

C57Bl/6J Enucleated Mice

Analysis of the infraslow connectivity matrix revealed significant alterations of both intrahemispheric (Supplemental figure 2A) and interhemispheric (Supplemental figure 2B) frequency distribution of correlation values. More negative intrahemispheric (Mann-Whitney's test, $p = 0.0028$) and positive interhemispheric (Mann-Whitney test, $p = 0.001$) correlations were observed in enucleated C57Bl/6J mice than in sighted controls.

ZRDBA Anophtalmic and Enucleated Mice

In ZRDBA mice, blindness did not significantly affect the frequency distribution of intrahemispheric correlations (Supplemental figure 2C; Kruskal-Wallis test, $p = 0.402$) in neither enucleated nor anophthalmic group, but the interhemispheric correlation distribution was significantly altered in the blind mice (Supplemental figure 2D; Kruskal-Wallis test, $p = 0.009$). Corrected multiple comparisons showed a shift towards more negative interhemispheric correlation in the enucleated mice ($p = 0.007$) than in sighted

mice. No significant difference was detected between sighted and anophthalmic mice ($p = 0.166$) nor between enucleated and anophtalmic mice ($p = 0.783$).

Alteration of the Connectivity Patterns

To explore differences in cortical network dynamics, we initially applied an uncorrected Welch's t-test ($p < 0.05$) to compare intra- and interhemispheric resting-state functional connectivity between sighted and early blind mice. This exploratory approach revealed a complex pattern of connectivity alterations, with both increases and decreases across various cortical regions (Figure 3).

C57Bl/6J Enucleated Mice (Figure 3A)

In C57Bl/6J enucleated mice, homotopic interhemispheric connectivity was increased across associative, visual, and auditory regions, with no observed decreases. Heterotopic interhemispheric connectivity also showed widespread enhancements, particularly between medial visual areas and somatosensory, motor, and associative cortices. Additionally, auditory area exhibited stronger interhemispheric connectivity with trigeminal-related and supplemental somatosensory, and lateral visual areas. In contrast, interhemispheric connectivity reductions were confined to motor–sensory interactions, notably between motor and sensory related (BC, AL and LM), and between V1 and lateral visual areas. Intrahemispheric connectivity showed notable increases between medial high-HVAs and associative, motor, and somatosensory cortices. In contrast, decreases were primarily confined to interactions between V1 and lateral visual, somatosensory, and associative regions.

ZRDBA Enucleated Mice (Figure 3B)

In ZRDBA enucleated mice, homotopic interhemispheric connectivity was unchanged. Heterotopic interhemispheric alterations were restricted to connections between medial visual areas and trigeminal-related, supplemental somatosensory, associative, auditory, and motor cortices. Intrahemispheric increases were limited between high-order visual areas (HVAS) and associative, auditory and somatosensory areas. Mild decreases were observed between dorsal column-related and associative regions.

ZRDBA Anophtalmic Mice (Figure 3C)

In ZRDBA anophthalmic mice, homotopic interhemispheric connectivity decreased in associative and motor cortices. Mild decreases of heterotopic connectivity were observed only between medial HVAs and trigeminal-related, supplemental somatosensory, associative, auditory, and motor areas, as well as between associative and motor regions. Increases of intrahemispheric connectivity were observed between HVAs and associative and somatosensory areas, with no observed reductions.

Circular Connectomes and Global Network Properties

The impact of neonatal enucleation and anophthalmia on the cortical connectome was evaluated with the application of a threshold dismissing correlations with absolute values below 0.3. This threshold minimized variability produced by weak or spurious edges (see grey boxes in supplementary figure 3). To assess large-scale network reorganizations, we quantified four global graph metrics: global efficiency, network density, total connectivity strength, and modularity. Global efficiency captures the average inverse shortest path length, reflecting the network's capacity for distributed information transfer (Rubinov and Sporns 2010). Density measures the proportion of suprathreshold connections. Total

strength represents the sum of all suprathreshold edge weights, indexing the network's functional robustness (van den Heuvel and Sporns 2011). Finally, Louvain modularity (Blondel *et al.* 2008) quantifies the extent of community structure, with higher values indicating stronger functional segregation.

Intrahemispheric Network Alterations

C57Bl/6J Enucleated Mice Connectome (Figure 4A-i)

In the enucleated C57Bl/6J mice, V1, lost connections with the somatosensory and auditory cortices. However, V1 established new connections with associative (RS) and motor (M1) V1 maintained its connectivity with HVAs. Enucleation also resulted in the loss of connections between lateral HVAs (AL, LM, and RL) and the medial HVA, PM. Conversely, connectivity increased between other medial HVAs (A and AM) and lateral HVAs (AL and LM).

Both lateral and medial HVAs exhibited an overall increase in suprathreshold connections, forming stronger links with other functional domains, including associative, auditory, motor, and somatosensory areas. More specifically, medial HVAs predominantly gained sensory connections from auditory and trigeminal-related somatosensory areas, whereas lateral HVAs primarily integrated sensory inputs from dorsal column-related somatosensory areas. Finally, associative areas, particularly RS, increased its connectivity with all functional domains (associative, auditory, somatosensory, motor and visual).

Global Network Metrics Alterations in Early Blind C57Bl/6J Mice (Figure 4B-i)

A Pillai's trace multivariate test on global network metrics revealed significant differences based on visual status in C57Bl/6J mice ($V = 0.872$, $F [4,4] = 6.828$, $p = 0.045$). Post hoc

Bonferroni corrected pairwise comparisons indicated significant increases in network density ($p = 0.050$), global efficiency ($p = 0.015$), and global strength ($p = 0.007$) in enucleated mice compared to sighted controls in the infraslow frequency range.

ZRDBA Enucleated Mice connectome (Figure 4A-ii)

In ZRDBA mice, enucleation impacted the cortical network structure differently than in C57Bl/6J mice. Indeed, enucleation did not alter V1 connectivity. However, lateral HVAs lost connections with associative, dorsal column-related somatosensory, and motor areas. In contrast, medial HVAs increased connectivity with trigeminal and dorsal column-related somatosensory areas, as well as with associative regions (AC and RS).

Other changes in connectivity were also observed in associative regions, AC lost connections with auditory areas, whereas RS strengthened its connections with dorsal column-related somatosensory areas.

ZRDBA Anophtalmic Mice connectome (Figure 4-iii)

In anophthalmic ZRDBA mice, V1 exhibited a reduction in connections with some somatosensory areas (S2, MO, NO and HL), but contrary to what's was observed in enucleated C57Bl/6J mice, it retained its connectivity with the barrel field cortex (BC) and auditory areas (AU and TEA).

Regarding medial HVAs, only PM showed connectivity losses, specifically with the anterior cingulate cortex (AC), the lateral HVAs (AL and LM), and motor area. However, concerning the medial HVAs, A, gained only a connection with RS, whereas AM, established several new connections with associative areas (AC and TEA), dorsal column-related (FL and HL) and trigeminal (MO and NO) somatosensory and auditory (AU) areas.

Additionally, connectivity between lateral HVA (RL) and dorsal column-related somatosensory (FL and TR) and associative (AC) areas were enhanced. In contrast, the other lateral HVAs (AL and LM), demonstrated a decreased connectivity with associative areas (AC and RS).

Associative cortices showed other alterations. Notably, AC and RS lost connections with forelimb-related somatosensory areas (FL) and RS gained connections with somatosensory areas (FL, MO and NO).

Global Network Metrics Alterations in Early Blind ZRDBA mice (Figure 4B-ii and 4B-iii)

No significant multivariate effect of visual status was observed in ZRDBA mice ($V = 0.385$, $F[8,18] = 0.536$, $p = 0.814$) for global network metrics. Additionally, Bonferroni-corrected pairwise comparisons revealed no significant differences when comparing sighted to enucleated mice, sighted to anophthalmic mice, or enucleated to anophthalmic mice.

Nodal Dynamics in Cortical Network Reorganization

To evaluate cortical network reorganization following early visual deprivation, we examined node-level changes using three graph-theoretical metrics: nodal efficiency, connectivity quality, and eigenvector centrality. These metrics respectively capture each region's capacity for global communication, local connection strength, and integration within highly connected substructures (Lohmann *et al.* 2010; Rubinov and Sporns 2010). Together, they provide a multidimensional profile of each node's functional prominence. Cross-metric ranking allowed for the qualitative identification of both the most and least influential nodes within each experimental group, as well as those demonstrating shifts in network influence following sensory deprivation. Nodes ranking highest across the

combination of all three metrics were designated as influential hubs, representing regions with the greatest overall network impact. Finally, nodes with scores exceeding one standard deviation above the group mean on any individual metric were classified as high-impact hubs and are illustrated with hatched bars in Figures 5–6. Based on their respective metrics, these hubs were categorized as efficient hubs (nodal efficiency), high-quality hubs (connectivity weight normalized by degree), and core hubs (eigenvector centrality).

Reallocation of Cortical Nodal Influences Following Neonatal Enucleation in C57Bl/6J Mice (Figure 5)

In sighted C57BL/6J mice, cortical network influence was predominantly driven by influential hubs such as auditory (AU), associative (TEA), and lateral visual areas (AL, LM), whereas associative (AC, RS), motor (M1), and medial visual (PM) regions exhibited the lowest influence. Following enucleation, the auditory cortex (AU) remained a key driver, accompanied by increased contributions from somatosensory regions (NO, TR, S2). In contrast, associative (AC) and motor (M1) areas persisted among the least influential nodes, now joined by visual regions (V1, AL). Overall, somatosensory (NO, TR) and medial visual areas (AM, PM) demonstrated the greatest increase in nodal influence after visual deprivation, while associative (TEA), lateral visual (AL, RL, LM), and primary visual (V1) areas showed the most pronounced decline. Multivariate analysis (Pillai's trace: $V = 0.851$, $F [57, 420] = 2.920$, $p < 0.001$) confirmed that neonatal enucleation induces widespread reorganization of cortical influence in C57Bl/6J.

Among visual cortices of sighted C57Bl/6J mice network, AL and V1 were labelled as efficient hubs, while AL and LM were considered as high-quality and core hubs. In enucleated network, all these areas demonstrated lost of their influential hubs'

qualification. Lateral (AL, LM, RL) and primary (V1) visual regions demonstrated the most prominent lost, with V1 exhibiting significant reductions in both efficiency ($p < 0.001$) and centrality ($p < 0.001$), while AL exhibited a decline in centrality ($p = 0.004$). RL also lost influence, with significant decreases in centrality ($p < 0.001$) and connectivity quality ($p = 0.020$). In contrast, medial HVAs (A, AM, PM) became more prominent. A showed increased quality ($p = 0.002$) and centrality ($p = 0.002$), while AM and PM exhibited significant gains across all three metrics (AM: quality ($p < 0.001$), centrality ($p < 0.001$), and efficiency ($p = 0.012$), PM: quality ($p = 0.005$), centrality ($p = 0.019$), and efficiency ($p = 0.044$)).

In sighted C57BL/6J mice, the barrel cortex (BC) was the only somatosensory region classified as an efficiency hub, whereas the supplemental somatosensory area (S2) qualified as a core hub. Notably, the nose region (NO) retained its designation as a core hub across both visual conditions. In enucleated C57Bl/6J mice, BC lost its efficiency hub status, while multiple somatosensory regions exhibited marked increases in network prominence (MO, S2, TR). The trunk (TR) region emerged as a key driver of network influence post-enucleation, showing robust increases across all three metrics ($p < 0.001$) and earning classification as efficient, high-quality and core hub. MO gained status as an efficiency hub through elevated nodal efficiency ($p = 0.013$) and connectivity quality ($p = 0.002$), while NO showed significant gains in efficiency ($p = 0.002$) and quality ($p < 0.001$), qualifying as both an efficient and high-quality hub. S2 maintained its role as a core hub and further gained designation as an efficient and high-quality hub, supported by increased efficiency ($p = 0.026$) and connection quality ($p = 0.001$). Hind limb (HL) regions exhibited consistent enhancements across all metrics—efficiency ($p = 0.001$), quality ($p = 0.004$),

and centrality ($p = 0.001$)—while the forelimb (FL) demonstrated increased quality ($p < 0.001$) and centrality ($p = 0.048$). The secondary motor cortex (M2) also gained influence in the enucleated mice cortical network, with significant elevations in efficiency ($p = 0.022$) and centrality ($p = 0.012$)

Of the associative and auditory cortices of sighted mice, the temporal association area (TEA) was classified as an efficient, high-quality, and core hub, indicating prominent network integration. However, in the enucleated mice, non-significant decreases across all metrics led to the loss of these classifications. In contrast, the primary auditory cortex (AU) maintained its status as a high-quality and core hub across both visual conditions. While the increase in nodal efficiency in enucleated C57Bl/6J mice did not reach significance, AU nonetheless gained designation as an efficient hub. Notably, AU exhibited a significant increase in connection quality in enucleated mice ($p = 0.002$). Furthermore, the retrosplenial cortex (RS) demonstrated strengthened network influence in enucleated mice, with significant increase in connection quality ($p < 0.001$) and centrality ($p = 0.007$).

Differential Reorganization of Cortical Nodal Influence in Anophthalmic and Enucleated ZRDBA Mice (Figure 6)

In the sighted ZRDBA mice, cortical network influence was primarily driven by auditory (AU), somatosensory (NO, S2), and lateral visual (AL) regions (influential hubs), while associative (RS), motor (M1, M2), and somatosensory (FL) areas exhibited the lowest influence. In the enucleated ZRDBA mice, influential hubs were composed of auditory (AU) and somatosensory (BC, S2) areas, while associative (AC), motor (M1, M2) and somatosensory (FL) areas were among the least influential. In the anophthalmic ZRDBA mice, auditory (AU) cortex also retained its influential hub rank, accompanied by

associative (TEA) and somatosensory (NO, S2) areas, whereas associative (RS) and somatomotor areas (FL, M1, and M2) ranked among the least influential. Cortical network comparison between sighted and enucleated ZRDBA mice revealed pronounced increases in nodal influence ranks for associative (RS) and visual (A, AM, RL) areas, and rank declines of associative (AC, TEA) and somatomotor areas (M1, M2, HL, MO). While comparing sighted and anophtalmic ZRDBA mice, associative (RS), medial visual (A, AM, PM) and somatosensory (TR) areas demonstrated the strongest influential rank gains, while associative (AC), motor (M2) and visual (RL, V1) areas showed the strongest influential rank reductions. Overall, early visual deprivation in ZRDBA mice induced significant although moderate cortical reorganization relative to C57BL/6J mice (Pillai's trace: $V = 0.716$, $F [114, 660] = 1.814$, $p < 0.001$).

In the visual cortex of sighted ZRDBA network, the anterolateral HVA (AL) was classified as both high-quality and core hub under sighted conditions. Although its high-quality hub status was lost in both enucleated and anophthalmic groups, its core hub designation was only lost in anophthalmic mice. Nonetheless, AL was maintained as an efficient hub in both early blindness models. Univariate analysis demonstrated that V1 centrality was significantly reduced in anophthalmic mice compared to enucleated animals ($p < 0.001$). Lateral and medial visual areas exhibited divergent trajectories in the anophthalmic but not in the enucleated ZRDBA mice. RL showed increased centrality in enucleated relative to sighted controls ($p = 0.010$), while both AL and RL showed reduced centrality in anophthalmic compared to sighted mice ($p = 0.001$ and $p < 0.001$). In contrast, medial HVAs, A and AM, demonstrated increased nodal influence. Centrality in AM was significantly elevated in both enucleated ($p = 0.016$) and anophthalmic ($p < 0.001$) mice,

while area A also showed a significant increase in centrality only in anophtalmic ($p < 0.001$) compared to sighted mice.

In the somatosensory and motor cortices of sighted ZRDBA network, S2 functioned as an efficient, high-quality and core hub, MO as an efficient and core hub, BC as an efficient hub and NO as a high-quality hub. In the enucleated ZRDBA mice, BC, NO, and S2 retained their classifications, whereas MO lost both efficient and core hub status. In the anophthalmic mice, BC and NO preserved all designations, while S2 and MO showed a selective loss of efficient hub classification. BC showed reduced centrality in anophthalmic compared to enucleated mice ($p = 0.012$). The most prominent reorganization was observed in the trunk-related area (TR), which exhibited significantly increased centrality in anophthalmic mice compared to both sighted and enucleated mice ($p < 0.001$). The hind limb (HL) region also showed a significant increase in centrality in anophthalmic relative to enucleated mice ($p < 0.001$).

In associative and auditory regions, the primary auditory cortex (AU) was the only area consistently classified as an efficient, high-quality and core hub across all visual conditions, underscoring its stable integrative role. The temporal association area (TEA) also functioned as an efficient hub in both sighted and anophthalmic ZRDBA mice. In enucleated animals, TEA exhibited significant reductions in connectivity quality ($p = 0.025$) and centrality ($p = 0.002$) compared to sighted controls. Notably, anophthalmic mice showed significantly elevated values in both metrics relative to enucleated counterparts (quality: $p = 0.027$; centrality: $p = 0.025$).

Differential Cortical Network Reorganization Following Neonatal Enucleation in C57BL/6J and ZRDBA Mice

Multivariate analysis (excluding anophthalmic ZRDBA mice) revealed a significant interaction between strain and visual status (Pillai's trace: $V = 0.064$, $F [3, 354] = 8.065$, $p < 0.001$). Enucleation led to strain-dependent changes in global efficiency ($p = 0.005$) and quality index ($p = 0.010$).

Neonatal enucleation produced distinct nodal influence patterns across strains. In C57BL/6J mice, reductions were observed in primary and lateral visual cortices, while medial visual, somatosensory, and motor areas showed increased influence. In ZRDBA mice, alterations were predominantly confined to visual cortical regions. Enucleated individuals from both strains demonstrated heightened centrality in high-order visual areas, whereas anophthalmic mice exhibited diminished nodal influence in lateral HVAs and enhanced connectivity in medial HVAs. Notably, the nodal influential profile of anophthalmic ZRDBA mice more closely aligned with that of enucleated C57BL/6J mice than with enucleated ZRDBA mice.

Functional Network Architecture and Intermodular Connectivity Following Early Blindness Across Mouse Strains

To investigate how early blindness altered the modular architecture of the cortical connectome, we applied Louvain community detection (Blondel *et al.* 2008) to identify modules based on intra- and interhemispheric correlation patterns. This method captures the balance between functional segregation and integration by maximizing the modularity. To quantify the similarity between modular structures between experimental groups, we used normalized mutual information (NMI), which measures the shared information between two partitions, scaled from 0 (no similarity) to 1 (identical structure). To assess the role of individual nodes within this modular framework, we computed three

complementary metrics: participation coefficient (PC), within-module centrality (WMC), and betweenness centrality (BeC). PC quantifies a node's connectivity across modules, identifying cross-community integrators (Guimerà and Nunes Amaral 2005). WMC reflects a node's importance within its own module, highlighting local hubs of cohesion. BeC measures how often a node lies on the shortest paths between others, indicating its role in global communication (van den Heuvel and Sporns 2011). Nodes with values exceeding one standard deviation above the mean plus for a given metric was classified as provincial hubs (WMC), connector nodes (PC), or bridging nodes (BeC), respectively. Together, these metrics provide a detailed view of how cortical regions contribute to intra- and intermodular connectivity in the context of congenital and early acquired blindness.

Neonatal Enucleation Induces Modular Reduction and Functional Reorganization of Structural Hubs in C57BL/6J Cortical Networks

In sighted C57Bl/6J mice, Louvain community detection revealed four distinct cortical intrahemispheric modules (Figure 7A). The first community (in blue) consisted solely of the associative region (RS) and had no structural hub. The second community (in yellow) included motor regions (M1, M2) and associative area (AC), anchored by M2 which served as both a provincial hub and a connector node; AC and M1 were also identified as connector nodes. The third community (in red) comprised dorsal column-related somatosensory areas (FL, HL, TR) and medial visual cortices (A, AM, PM). It was centered around TR, identified as both a provincial and bridging hub, while PM served as a connector node. The fourth community (in purple) encompassed trigeminal-related regions (BC, MO, NO), supplementary somatosensory area (S2), primary visual cortex (V1),

lateral visual areas (AL, LM, RL), auditory region (AU), and associative cortex (TEA). AL and AU were identified as provincial hubs, with AU also acting as a bridging node.

In enucleated C57Bl/6J mice (Figure 7B), the cortical network reorganized into three communities. The first community (in yellow) included somatosensory regions (MO, NO, S2), associative area (AC), and motor regions (M1, M2). NO emerged as a provincial hub, a connector, and a bridging node, highlighting its prominent role in local and intermodular coordination. AC, MO, and M2 were also identified as connector nodes. The second community (in red) included dorsal column-related somatosensory areas (FL, HL, TR), medial visual cortices (A, AM, PM), primary visual cortex (V1), and associative region (RS). AM and TR were identified as provincial hubs, with AM also serving as a bridging node and RS as a connector node. The third community (in purple) was composed of the somatosensory region (BC), lateral visual cortices (AL, LM, RL), auditory area (AU), and the associative cortex (TEA). AU was identified as both a provincial hub and a bridging node.

Cortical Community Reorganization and Node Role Shifts Following Enucleation in C57Bl/6J Mice

Overall, NMI between cortical networks communities of sighted and enucleated mice reached 57.4%. Multivariate analysis revealed significant effects of enucleation on nodal structural metrics, including within-module centrality, participation coefficients, and betweenness centrality, with a strong interaction between visual status and cortical region (Pillai's trace: $V = 1.274$, $F [57, 420] = 5.436$, $p < 0.001$). Nearly all regions were significantly affected (except for HL), reflecting a redistribution of local and intermodular influence and a profound reorganization of cortical network.

Univariate statistical analysis further highlighted significant nodal changes within the structural hubs of the enucleated C57Bl/6J mice cortical network. Among provincial hubs, AU and TR remained stable, whereas M2 ($p < 0.001$) and AL ($p = 0.003$) lost their hub designation. Conversely, AM ($p = 0.007$) and NO ($p < 0.001$) emerged as new provincial hubs, indicating an increased involvement of somatosensory and medial visual areas in cortical processing. Connector node dynamics followed a similar trend, with AC and M2 maintaining their roles, while MO ($p = 0.022$), NO ($p < 0.001$), and RS ($p = 0.026$) were newly classified as connector nodes. Although M1 and PM lost their connector status, their changes in participation coefficients did not reach statistical significance. Modifications in bridging nodes further illustrated the network's reorganization. AU preserved its bridging role, whereas TR showed a nonsignificant increase in betweenness centrality but lost its bridging node status. In contrast, AM ($p = 0.004$) and NO ($p < 0.001$) no longer served as bridging nodes due to significant reductions in betweenness centrality. These results point to a shift in long-range cortical communication, favoring distributed integration over centralized bottlenecks. To summarize, nodal structural reorganization supported by statistical analysis included a significant loss of provincial hub status for AL and M2, while AM and NO significantly emerged as new provincial hubs. Additionally, MO, NO, and RS gained connector node classification, each driven by statistically significant increases in participation coefficients. AM and NO also transitioned into bridging node roles, supported by significant elevations in betweenness centrality.

<u>Visual Deprivation Models Reshape Cortical Architecture Through Modular Reduction and Nodal Structural Reclassification in ZRDBA Mice</u>

In sighted ZRDBA mice (Figure 8A), Louvain analysis identified four distinct cortical communities. An anterior community (in yellow) was composed of AC and M2 and both were labelled as connector nodes. A second community (in blue) integrated dorsal column related somatosensory (FL, HL, TR) and motor (M1) areas. In this community, TR was identified as both connector and bridging node, while HL was also considered as a bridging node. A third community (in purple) incorporated trigeminal-related (BC, MO, NO) and supplemental somatosensory (S2), lateral (AL, LM, RL) and primary visual (V1) and auditory (AU) areas. In terms of nodal structure, AU and S2 functioned as provincial hubs, while AU was also identified as a bridging node. Additionally, AL was also considered as a bridging node. Finally, a fourth community (in red) was composed of associative (RS) and medial visual (A, AM, PM) areas. In this community, AM was a provincial node, while PM was a bridging node.

In the enucleated ZRDBA mice (Figure 8B), the cortical network was restructured into three communities. A first community (in yellow), which incorporated the somatomotor (FL, M1, M2) areas, in which M2 qualified as a provincial hub. Additionally, AC, FL and M1 were considered as connector nodes. A second community (in red) contained associative (RS), dorsal column-related somatosensory (HL, TR) and medial visual (A, AM, PM) areas. AM had both a provincial hub and a bridging node function. HL and TR were also considered as bridging nodes, additionally, HL was also qualified as a connector node. A third community (in purple) encompassed associative (TEA), auditory (AU), trigeminal-related (BC, MO, NO) and supplemental somatosensory (S2) and lateral (AL, LM, RL) and primary visual (V1). AU acted as both a provincial hub and a bridging node.

In anophthalmic ZRDBA mice (Figure 8C), we observed three distinct cortical communities. A first community (in yellow), having a structure similar as to sighted mice was composed of AC and M2, which were both connector nodes. A second community (in purple) comprised associative (TEA), auditory (AU), trigeminal (BC, MO, NO) and supplemental somatosensory (S2) and lateral visual (AL and LM) areas with AU and S2 as provincial hubs. A third community (in red) was composed by associative (RS), motor (M1), dorsal column related somatosensory (FL, HL and TR) and visual (A, AM, PM, RL and V1) areas. AM served as a provincial hub alongside HL and TR. Together with TR, both AM and HL also acted as bridging nodes. Additionally, M1 and HL functioned as connector hubs.

Cortical Community Structure and Nodal Function Modulation Following Early Blindness Across Distinct Visual Conditions in ZRDBA mice

Comparative analysis of cortical network communities revealed moderate overlap in structural organization across visual conditions. In this mice strain, NMI values were 79.2% (sighted vs. enucleated), 64.1% (sighted vs. anophthalmic), and 56.2% (anophthalmic vs. enucleated). Multivariate analysis demonstrated significant effects of enucleation on nodal metrics including within-module centrality, participation coefficients, and betweenness centrality, with a robust interaction between visual status and cortical region (Pillai's trace: $V = 1.079$, $F\ [114, 660] = 3.254$, $p < 0.001$). Early blindness significantly impacted associative (RS, TEA), motor (M2), somatosensory (BC, FL, HL, TR), visual (A, AL, PM, RL, V1), and auditory (AU) regions.

Univariate analysis comparing sighted and enucleated ZRDBA mice revealed notable shifts in nodal structural function across cortical communities. Among the identified provincial

hubs, AU and AM maintained stable roles across conditions. M2 emerged as a new provincial hub, marked by a significant increase in WMC ($p = 0.001$). Conversely, S2 lost its hub status despite exhibiting no significant change in WMC. For the connector nodes, AC and M1 retained their roles, with participation coefficients remaining unchanged. In contrast, M2 and TR lost their connector node classification, exhibiting a significant decrease in the participation coefficient (both $p < 0.001$). Additionally, FL and HL gained connector node status, with FL showing a significant increase in participation coefficient ($p = 0.010$), whereas HL's rise did not reach statistical significance. For the bridging nodes, AU, HL and TR maintained their bridging roles, with betweenness centrality showing no significant changes. PM and AL, however, lost their classification as bridging nodes, though their betweenness centrality decreases were not statistically significant. AM, in contrast, gained bridging node status, yet this shift was not accompanied by a significant betweenness centrality increase. To summarize, nodal structural reorganization supported by statistical analysis between sighted and enucleated mice included M2's dual shift—emerging as a provincial hub while losing its connector node status. TR also lost connector classification due to a significant decline in participation coefficients, whereas FL gained connector node status, driven by a significant increase in participation coefficients.

Univariate analysis comparing sighted and anophthalmic ZRDBA mice revealed key shifts in nodal roles within cortical communities. Among provincial hubs, AM, AU and S2 maintained their hub status, showing no significant changes in WMC, while TR and A gained provincial hub classification, though only the WMC of TR was significantly increased ($p < 0.001$). Changes in connector nodes followed a similar trend, with AC, M1, and M2 retaining their roles, as their participation coefficients remained unchanged (except

for M2; $p = 0.025$). In contrast, TR lost its connector node classification, through a participation coefficient significant decrease ($p < 0.001$). In addition, HL gained the connector node status, yet its participation coefficient increase did not reach statistical significance. HL and TR consistently retained their roles as bridging nodes, with no significant changes of their betweenness centrality score. AU and PM lost their bridging status, although declines in betweenness centrality were not statistically significant. AL also lost its classification, accompanied by a significant reduction in betweenness centrality ($p = 0.033$). AM gained bridging node status, though this reclassification was not supported by a significant increase in betweenness centrality.

To summarize, statistically supported nodal structural reorganization between sighted and anophtalmic mice included TR's emergence as a provincial hub alongside its loss of connector status, and AL's loss of bridging node classification driven by a significant decrease in betweenness centrality.

Univariate analysis comparing anophthalmic and enucleated ZRDBA mice revealed key differences in nodal roles across cortical communities. Among provincial hubs, AU and AM maintained their classification, with no significant changes in WMC. Conversely, A, TR and S2 lost their provincial hub designation, though their WMC reductions were not statistically significant, while M2 gained provincial hub status without significant decrease of WMC. Having stable participation coefficients, AC, M1, and HL remained connector nodes. In contrast, M2 lost its connector node status without a significant decrease in participation coefficients, while FL emerged as a new connector node with a statistically significant increase in participation coefficient ($p < 0.001$). For the bridging nodes, AM, HL and TR maintained their function with no significant alterations in betweenness

centrality, whereas AU gained the classification, though its increase in betweenness centrality was not significant. Overall, the only statistically supported structural hub alteration between anophthalmia and enucleation was the emergence of FL as a connector node, driven by increased participation.

Visual Deprivation and Genetic Background Synergistically Reshape Cortical Network Modularity

Enucleated C57BL/6J and both early blind ZRDBA mice showed reduced cortical modularity, with the number of communities dropping from four to three, alongside increased intermodular connectivity. Between sighted C57BL/6J and ZRDBA mice NMI reached 77.6% but declined to 49.8% between their enucleated counterparts, indicating greater structural divergence after early enucleation. Multivariate analysis revealed a significant interaction between strain and visual status on network topology (Pillai's trace: $V = 0.156$, $F [3, 354] = 21.780$, $p < 0.001$). Although WMC and betweenness centrality did not differ significantly across strains, participation coefficient values were significantly elevated in C57BL/6J mice ($p < 0.001$), suggesting stronger intermodular integration compared to ZRDBA.

Discussion

Alteration of the infraslow oscillation activity

Our findings demonstrate that early visual deprivation altered the spectral dynamics of cortical activity, particularly in the infraslow oscillation (ISO) range, across both mouse strains studied. In C57Bl/6J mice, neonatal enucleation led to a generalized increase in ISO power, most prominently in associative, dorsal column related somatosensory and medial

visual cortices. In contrast, enucleated ZRDBA mice showed more limited enhancements, primarily in auditory and trigeminal-related somatosensory cortices. These strain-specific patterns suggest distinct forms of large-scale cortical reorganization in response to early loss of vision.

Prior studies have reported that sensory deprivation alters ISOs in both mice and humans (Burton *et al.* 2014; Wang *et al.* 2014; Heine *et al.* 2015; Kraft *et al.* 2017). ISOs are recognized as markers of intrinsic large-scale cortical connectivity and excitability (Vanhatalo *et al.* 2004; Fox *et al.* 2005; Fox *et al.* 2006; Power *et al.* 2011; Mitra *et al.* 2014; Sforazzini *et al.* 2014; Mitra *et al.* 2015).

Our data shows a similar spatial profile of ISO power increases in the enucleated C57Bl/6J and in the anophthalmic ZRDBA mice which is distinct form that seen in the enucleated ZRDBA mice. This could reflect the genetic contribution to cortical plasticity. Specifically, the amplitude of ocular dominance shift was reported to be twofold greater in C57Bl/6J compared to the DBA mice (Heimel *et al.* 2008). Monocular deprivation is widely used to study experience-dependant cortical plasticity and has a strong genetic background and heritability (Heimel *et al.* 2008). As ZRDBA mice were produced by crossing DBA with ZRDCT/An strains (Chase and Chase 1941; Chase 1942, 1944; Tucker *et al.* 2001), they likely inherited more limited cortical plasticity from DBA mice. Additionally, within the ZRDBA strain itself, we observed distinct ISO profiles between anophthalmic and enucleated animals. These differences are consistent with our previous observations of strain differences in the size and growth of visual cortex following enucleation and anophthalmia in the C57BL6J mice and the ZRDCT/An mouse (Massé *et al.* 2014).

Human studies bear both similarities and differences with what we observe here in blind mice. In congenitally blind individuals, reorganization affects visual, auditory, frontal, and retrosplenial regions (Lubinus *et al.* 2021), consistent with the territories modulated in our murine models. However, humans show more extensive spectral changes, including increased theta and beta power and reduced alpha activity (Noebels *et al.* 1978; Kriegseis *et al.* 2006; Schepers *et al.* 2012; Hawellek *et al.* 2013; Schubert *et al.* 2015; Gudi-Mindermann *et al.* 2018; Rimmele *et al.* 2019). In contrast, our recordings revealed changes predominantly below 4 Hz, concentrated in the infraslow and delta bands. Although some signal extended into theta and alpha ranges, no consistent group differences emerged beyond 4 Hz. This discrepancy may be attributed to species-specific plasticity profiles, but methodological limitations such as the slow kinetics of calcium indicators (GCaMP6s) likely contributed as well. Additionally, our data does not capture the full spectral range, notably excluding beta and gamma oscillations.

The functional reorganization observed in our study is likely supported by homeostatic plasticity mechanisms engaged in response to early sensory deprivation. Experimental evidence has shown that blindness induces synaptic scaling, alterations in excitation–inhibition balance, and heightened cortical excitability (Keck *et al.* 2013; Gainey and Feldman 2017). In rodents, these adaptations include potentiated thalamocortical and intracortical connectivity in spared sensory pathways (Gao *et al.* 2010; Gao *et al.* 2014; Petrus *et al.* 2014; Petrus *et al.* 2015; Ewall *et al.* 2021), in agreement with reallocation of cortical processing. Moreover, our results further documents that such changes shape both local circuitry and whole-brain functional connectivity (Lambo and Turrigiano 2013; Hellyer *et al.* 2016; Rocha *et al.* 2018).

Alteration of interhemispheric functional connectivity

Our analysis revealed strain-specific patterns of cortical network reorganizations following early visual deprivation. In C57Bl/6J enucleated mice, we observed widespread increases in both heterotopic and homotopic interhemispheric connectivity of associative, auditory, and visual regions, suggesting wide ranging consequences of visual deprivation, well beyond the realm of visual cortical areas. ZRDBA enucleated mice exhibited subtler changes, with stable homotopic connectivity and selective heterotopic enhancements, particularly involving medial higher visual areas. In contrast, ZRDBA anophthalmic mice showed reduced homotopic connectivity in associative and motor cortices, while maintaining similar heterotopic enhancements of medial HVAs as observed in enucleated ZRDBA mice.

The widespread increases in homotopic and heterotopic interhemispheric connectivity in C57Bl/6J enucleated mice, notably involving associative and auditory mirror findings in congenitally blind humans, in whom non-visual networks exhibit enhanced cross-hemispheric integration (Bedny *et al.* 2011; Burton *et al.* 2014). However, increased connectivity within visual cortices diverges from human data (Bauer *et al.* 2017), potentially reflecting species-specific effects. Interestingly, spontaneous neural activity in blind individuals has been shown to synchronize more strongly across hierarchically related visual areas than across homotopic regions, suggesting a reorganization favoring cortico-cortical pathways within each hemisphere (Butt *et al.* 2015). Additionally, blindness has been associated with broader, fine-scale functional coupling within striate cortex, suggesting a redistribution of intrinsic connectivity toward non-visual domains (Butt *et al.* 2013).

Conversely, the more subtle and targeted reorganization seen in ZRDBA enucleated mice, marked by stable homotopic connectivity and selective heterotopic increases, resembles the nuanced connectivity patterns described in other human studies (Qin *et al.* 2013; Bridge and Watkins 2019), which highlight localized adaptations and maintenance of structural integrity even in the absence of vision.

Importantly, the reduced homotopic connectivity in ZRDBA anophthalmic mice, particularly within associative and motor cortices, reflects diminished interhemispheric synchrony and structural alterations in visual callosal pathways reported in humans (Shimony *et al.* 2006; Watkins *et al.* 2012; Tomaiuolo *et al.* 2014; Bauer *et al.* 2017; Hou *et al.* 2017). MRI studies report thinning of the posterior corpus callosum in early blind individuals, which supports reduced visual interhemispheric transfer (Ptito *et al.* 2008; Lepore *et al.* 2010), and increases in the anterior and mid-body regions suggesting an enhanced integration across frontal, somatosensory, and auditory areas (Ptito *et al.* 2008; Tomaiuolo *et al.* 2014). This reorganization suggests that visual cortices may reduce their reliance on interhemispheric exchange while strengthening connections with non-visual modalities. However, other reports found no callosal changes in early blind or anophthalmic individuals (Bock *et al.* 2013), indicating variability across cohorts. In contrast, animal models consistently show disrupted development of visual callosal projections following deprivation paradigms such as dark rearing, eyelid suture, or optic chiasm sectioning (Lund and Mitchell 1979; Innocenti *et al.* 1985; Frost and Moy 1989; Boire *et al.* 1995). Conversely, early enucleation or strabismus may preserve exuberant projections by limiting pruning (Berman and Payne 1983; Milleret 1994). In rodents, enucleation and anophthalmia often produce broader callosal neuron distributions,

extending beyond the typical boundaries of primary and extrastriate cortices (Olavarria and van Sluyters 1984; Rhoades *et al.* 1984; Olavarria *et al.* 1987; Olavarria *et al.* 1988; Olavarria and Li 1995).

Cortical Connectivity Modifications Following Early Visual Deprivation

Resting-state functional connectivity analyses revealed significant intrahemispheric cortical reorganization in C57Bl/6J mice following early enucleation, aligning with their documented enhanced neuroplasticity (Heimel *et al.* 2008). In contrast, ZRDBA mice showed minimal network alteration, consistent with their lower capacity for plastic remodeling.

Notably, anophthalmic ZRDBA mice, lacking retinal development and spontaneous prenatal retinal activity, exhibited cortical connectivity patterns resembling those of enucleated C57Bl/6J mice. This convergence implies that, in the absence of early retinal signaling, cortical networks default to genetically programmed configurations.

Enucleated ZRDBA mice retain residual prenatal retinal activity but fail to show substantial reorganization, suggesting this limited activity either lacks the strength to override pre-established spontaneous wiring or sufficiently preserves thalamocortical integrity. In contrast, complete absence of afferent retinal input in anophthalmic ZRDBA animals has a more pronounced effect on cortical development.

These results underscore a multifactorial influence, genetic background, developmental timing, and prenatal spontaneous activity, in shaping cortical reorganization trajectories. The C57Bl/6J strain, owing to its high plastic potential, enucleation reshapes cortical

networks in a manner that converges toward genetically anchored configurations like those observed in congenitally blind ZRDBA mice.

Importantly, cortical area V1 in anophthalmic ZRDBA mice reorganizes similarly to that in enucleated C57Bl/6J animals, reinforcing the critical role of early retinal activity in thalamocortical circuit formation (Blankenship and Feller 2010; Ackman *et al.* 2012). Because enucleation occurs postnatally, after retinogeniculate pathway development, resulting changes affect predominantly cortico-cortical interactions.

These strain-specific and developmental differences have translational relevance, echoing findings on genetically mediated plasticity (Kaschube *et al.* 2002; Missitzi *et al.* 2011) and contributing to the understanding of variability in human responses to sensory deprivation. In anophthalmic mice, reallocation of subcortical projections might predominate (Rhoades *et al.* 1985; Chabot *et al.* 2008), whereas enucleation might favor cortical reorganization involving associative and higher-order visual areas.

Area-Specific Plasticity: Insights from V1

Changes in connectivity were not uniform across the cortex. Notably, V1 in enucleated C57Bl/6J mice exhibited diminished intrahemispheric connectivity with somatosensory and auditory cortices, but increased connectivity with associative regions, such as the retrosplenial cortex. This reorganization echoes findings in early blind humans, where V1 becomes more tightly coupled to multimodal association areas and less connected to non-visual primary sensory and motor cortices (Burton *et al.* 2014; Bauer *et al.* 2017; Abboud and Cohen 2019).

This shift may be driven by V1's newly acquired responsiveness to non-visual stimuli. Functional activation of the visual cortex by tactile and auditory inputs has been consistently reported in blind subjects (Hyvarinen *et al.* 1981; Roder *et al.* 1996; Sadato *et al.* 1996; Cohen *et al.* 1997; Kujala *et al.* 1997; Sadato *et al.* 1998; Weeks *et al.* 2000) and is often interpreted as evidence of enhanced crossmodal connectivity (Wittenberg *et al.* 2004; Petrus *et al.* 2014; Petrus *et al.* 2015).

Other studies, however, document a decrease in connectivity between V1 and spared sensory cortices (Liu *et al.* 2007; Yu *et al.* 2008; Shu *et al.* 2009), revealing the complexity of crossmodal plasticity and its dependence on developmental timing and network architecture.

Higher Visual Areas as Dynamic Network Hubs

In our study, one of the most compelling observations was the emergence of medial HVAs, particularly area AM, as influential and structural hub within the reorganized cortical network of enucleated C57Bl/6J mice. These regions exhibited increased functional connectivity with non-visual sensory cortices, suggesting that medial HVAs play a central integrative role following early sensory loss. In contrast, primary and lateral visual cortices showed reduced nodal influence, highlighting a functional divergence among HVAs that may reflect differential specialization in crossmodal processing.

Anatomical studies in sighted mice support our findings, demonstrating that HVAs, particularly PM, LM, and AM, as well as the associative retrosplenial area, provide robust top-down projections to V1 (Oh *et al.* 2014; Zingg *et al.* 2014; Morimoto *et al.* 2021). Additionally, anatomical studies in visually deprived mice confirm that these projections

remain structurally intact and may be functionally strengthened following sensory loss. This would be in agreement with the connectivity constrained experience dependency hypothesis (Saccone *et al.* 2024). In fact, it was demonstrated that HVAs maintain top-down projections to V1 in enucleated mice (Laramée *et al.* 2011; Gilissen and Arckens 2021) and that V1 receives direct inputs from auditory and somatosensory in both enucleated and anophtalmic mice (Charbonneau *et al.* 2012), suggesting that crossmodal integration may rely on pre-existing corticocortical pathways.

Human studies support this organizational framework across both sighted and blind individuals. In sighted subjects, structural imaging has revealed intrinsic anatomical connectivity between visual and non-visual sensory cortices, supporting the potential for multisensory integration even in the presence of intact vision (Foxe and Schroeder 2005; Macaluso and Driver 2005; Macaluso 2006; Ricciardi, Bonino*, et al.* 2014). In blind individuals, this system undergoes experience-dependent reorganization, with increased structural and functional coupling between occipital areas and auditory or tactile regions (Noppeney *et al.* 2005; Collignon *et al.* 2006; Collignon *et al.* 2009; Klinge *et al.* 2010; Bedny *et al.* 2011; Collignon *et al.* 2011; Collignon *et al.* 2013). Activation of the occipital cortex during tactile and auditory tasks appears to be driven primarily by top-down feedback from dorsal and ventral HVAs (Ricciardi, Tozzi*, et al.* 2014; Murphy *et al.* 2016), while direct connections from primary sensory cortices to V1 tend to diminish (Liu *et al.* 2007; Ortiz-Terán *et al.* 2017). These pathways suggest that HVAs and associative regions are strategically positioned to influence V1 activity, even in the absence of visual input, reinforcing their potential importance in cross-modal recruitment of V1.

Retrosplenial Cortex: A Consistent Integrative Node

Across all models, the retrosplenial cortex (RS) consistently gained influence within the functional network. Long considered a hub for spatial processing, the RS is increasingly recognized for its role in multisensory and unimodal integration (Hindley *et al.* 2014; Fournier *et al.* 2020; Alexander *et al.* 2023). Its elevated centrality in enucleated mice suggests that associative regions play a crucial role in network dynamics after sensory loss. This supports the hypothesis that existing cortico-cortical projections are recruited during crossmodal plasticity (Smolders *et al.* 2016; Barnes *et al.* 2022), with RS serving as a bridge between deprived and active sensory regions. These results also support that the connectivity constrained hypothesis (Saccone *et al.* 2024) also applies to our murine models of visual deprivation.

Conclusion

In conclusion, our study demonstrates that neonatal sensory deprivation profoundly alters cortical connectivity, with distinct patterns of reorganization depending on the timing of sensory loss and genetic background. The differential plasticity observed between C57Bl/6J and ZRDBA mice highlight the interplay between genetic factors and sensory experience in shaping cortical networks. By elucidating the mechanisms underlying crossmodal reorganization and the role of higher visual areas, our findings provide novel insights into the adaptive capacity of the brain following sensory deprivation.

While our study provides important insights into the large-scale cortical reorganization following neonatal sensory deprivation, a more granular understanding of the underlying cellular mechanisms is needed. Specifically, the role of distinct neuronal populations, excitatory and inhibitory, in these processes remains largely unexplored. Investigating how sensory deprivation alters the activity and connectivity of specific excitatory populations,

such as pyramidal neurons, and inhibitory populations, such as interneurons, will be pivotal in elucidating the dynamics of cortical reorganization. Furthermore, it is crucial to explore how these alterations affect synaptic plasticity, neurotransmitter release, and the fine-tuned balance between excitation and inhibition that is critical for maintaining network stability.

REFERENCES

Abboud S, Cohen L. 2019. Distinctive Interaction Between Cognitive Networks and the Visual Cortex in Early Blind Individuals. Cereb Cortex. 29:4725-4742.

Ackman JB, Burbridge TJ, Crair MC. 2012. Retinal waves coordinate patterned activity throughout the developing visual system. Nature. 490:219-225.

Alexander AS, Place R, Starrett MJ, Chrastil ER, Nitz DA. 2023. Rethinking retrosplenial cortex: Perspectives and predictions. Neuron. 111:150-175.

Amedi A, Floel A, Knecht S, Zohary E, Cohen LG. 2004. Transcranial magnetic stimulation of the occipital pole interferes with verbal processing in blind subjects. Nat Neurosci. 7:1266-1270.

Andelin AK, Olavarria JF, Fine I, Taber EN, Schwartz D, Kroenke CD, Stevens AA. 2018. The Effect of Onset Age of Visual Deprivation on Visual Cortex Surface Area Across-Species. Cerebral Cortex. 29:4321-4333.

Andermann ML, Kerlin AM, Roumis DK, Glickfeld LL, Reid RC. 2011. Functional Specialization of Mouse Higher Visual Cortical Areas. Neuron. 72:10.1016/j.neuron.2011.1011.1013.

Anton-Bolanos N, Sempere-Ferrandez A, Guillamon-Vivancos T, Martini FJ, Perez-Saiz L, Gezelius H, Filipchuk A, Valdeolmillos M, Lopez-Bendito G. 2019. Prenatal activity from thalamic neurons governs the emergence of functional cortical maps in mice. Science. 364:987-990.

Barnes SJ, Keller GB, Keck T. 2022. Homeostatic regulation through strengthening of neuronal network-correlated synaptic inputs. eLife. 11:e81958.

Bauer CM, Hirsch GV, Zajac L, Koo BB, Collignon O, Merabet LB. 2017. Multimodal MR-imaging reveals large-scale structural and functional connectivity changes in profound early blindness. PLoS One. 12:e0173064.

Bedny M, Pascual-Leone A, Dodell-Feder D, Fedorenko E, Saxe R. 2011. Language processing in the occipital cortex of congenitally blind adults. Proc Natl Acad Sci U S A. 108:4429-4434.

Berman NE, Payne BR. 1983. Alterations in connections of the corpus callosum following convergent and divergent strabismus. Brain Res. 274:201-212.

Blankenship AG, Feller MB. 2010. Mechanisms underlying spontaneous patterned activity in developing neural circuits. Nat Rev Neurosci. 11:18-29.

Blondel VD, Guillaume J-L, Lambiotte R, Lefebvre E. 2008. Fast unfolding of communities in large networks. Journal of Statistical Mechanics: Theory and Experiment. 2008:P10008.

Bock AS, Saenz M, Tungaraza R, Boynton GM, Bridge H, Fine I. 2013. Visual callosal topography in the absence of retinal input. Neuroimage. 81:325-334.

Boire D, Morris R, Ptito M, Lepore F, Frost DO. 1995. Effects of neonatal splitting of the optic chiasm on the development of feline visual callosal connections. Exp Brain Res. 104:275-286.

Bonaventure N, Karli P. 1968. [Appearance in the visual cortex of evoked potentials of auditive origin in mice deprived of photoreceptors]. J Physiol (Paris). 60 Suppl 2:407.

Bridge H, Watkins KE. 2019. Structural and functional brain reorganisation due to blindness: The special case of bilateral congenital anophthalmia. Neuroscience & Biobehavioral Reviews. 107:765-774.

Burton H, Snyder AZ, Raichle ME. 2014. Resting state functional connectivity in early blind humans. Front Syst Neurosci. 8:51.

Butt OH, Benson NC, Datta R, Aguirre GK. 2013. The Fine-Scale Functional Correlation of Striate Cortex in Sighted and Blind People. The Journal of Neuroscience. 33:16209-16219.

Butt OH, Benson NC, Datta R, Aguirre GK. 2015. Hierarchical and homotopic correlations of spontaneous neural activity within the visual cortex of the sighted and blind. Front Hum Neurosci. 9:25.

Cang J, Rentería RC, Kaneko M, Liu X, Copenhagen DR, Stryker MP. 2005. Development of precise maps in visual cortex requires patterned spontaneous activity in the retina. Neuron. 48:797-809.

Chabot N, Charbonneau V, Laramée ME, Tremblay R, Boire D, Bronchti G. 2008. Subcortical auditory input to the primary visual cortex in anophthalmic mice. Neurosci Lett. 433:129-134.

Chabot N, Robert S, Tremblay R, Miceli D, Boire D, Bronchti G. 2007. Audition differently activates the visual system in neonatally enucleated mice compared with anophthalmic mutants. European Journal of Neuroscience. 26:2334-2348.

Chan KY, Jang MJ, Yoo BB, Greenbaum A, Ravi N, Wu WL, Sánchez-Guardado L, Lois C, Mazmanian SK, Deverman BE, Gradinaru V. 2017. Engineered AAVs for efficient noninvasive gene delivery to the central and peripheral nervous systems. Nat Neurosci. 20:1172-1179.

Charbonneau V, Laramée ME, Boucher V, Bronchti G, Boire D. 2012. Cortical and subcortical projections to primary visual cortex in anophthalmic, enucleated and sighted mice. Eur J Neurosci. 36:2949-2963.

Chase HB. 1942. Studies on an Anophthalmic Strain of Mice. III. Results of Crosses with Other Strains. Genetics. 27:339-348.

Chase HB. 1944. Studies on an Anophthalmic Strain of Mice. IV. a Second Major Gene for Anophthalmia. Genetics. 29:264-269.

Chase HB, Chase EB. 1941. Studies on an anophthalmic strain of mice I. Embryology of the eye region. Journal of Morphology. 68:279-301.

Cohen LG, Celnik P, Pascual-Leone A, Corwell B, Falz L, Dambrosia J, Honda M, Sadato N, Gerloff C, Catala MD, Hallett M. 1997. Functional relevance of cross-modal plasticity in blind humans. Nature. 389:180-183.

Collignon O, Davare M, Olivier E, De Volder AG. 2009. Reorganisation of the right occipito-parietal stream for auditory spatial processing in early blind humans. A transcranial magnetic stimulation study. Brain Topogr. 21:232-240.

Collignon O, Dormal G, Albouy G, Vandewalle G, Voss P, Phillips C, Lepore F. 2013. Impact of blindness onset on the functional organization and the connectivity of the occipital cortex. Brain. 136:2769-2783.

Collignon O, Lassonde M, Lepore F, Bastien D, Veraart C. 2006. Functional Cerebral Reorganization for Auditory Spatial Processing and Auditory Substitution of Vision in Early Blind Subjects. Cerebral Cortex. 17:457-465.

Collignon O, Vandewalle G, Voss P, Albouy G, Charbonneau G, Lassonde M, Lepore F. 2011. Functional specialization for auditory-spatial processing in the occipital cortex of congenitally blind humans. Proc Natl Acad Sci U S A. 108:4435-4440.

Colonnese MT. 2014. Rapid developmental emergence of stable depolarization during wakefulness by inhibitory balancing of cortical network excitability. J Neurosci. 34:5477-5485.

D'Souza RD, Wang Q, Ji W, Meier AM, Kennedy H, Knoblauch K, Burkhalter A. 2022. Hierarchical and nonhierarchical features of the mouse visual cortical network. Nat Commun. 13:503.

Dupont E, Hanganu IL, Kilb W, Hirsch S, Luhmann HJ. 2006. Rapid developmental switch in the mechanisms driving early cortical columnar networks. Nature. 439:79-83.

Ewall G, Parkins S, Lin A, Jaoui Y, Lee H-K. 2021. Cortical and Subcortical Circuits for Cross-Modal Plasticity Induced by Loss of Vision. Frontiers in Neural Circuits. 15.

Finneran DJ, Njoku IP, Flores-Pazarin D, Ranabothu MR, Nash KR, Morgan D, Gordon MN. 2021. Toward Development of Neuron Specific Transduction After Systemic Delivery of Viral Vectors. Frontiers in Neurology. 12.

Fournier DI, Monasch RR, Bucci DJ, Todd TP. 2020. Retrosplenial cortex damage impairs unimodal sensory preconditioning. Behav Neurosci. 134:198-207.

Fox MD, Corbetta M, Snyder AZ, Vincent JL, Raichle ME. 2006. Spontaneous neuronal activity distinguishes human dorsal and ventral attention systems. Proc Natl Acad Sci U S A. 103:10046-10051.

Fox MD, Snyder AZ, Vincent JL, Corbetta M, Van Essen DC, Raichle ME. 2005. The human brain is intrinsically organized into dynamic, anticorrelated functional networks. Proc Natl Acad Sci U S A. 102:9673-9678.

Foxe JJ, Schroeder CE. 2005. The case for feedforward multisensory convergence during early cortical processing. NeuroReport. 16:419-423.

Frost DO, Moy YP. 1989. Effects of dark rearing on the development of visual callosal connections. Exp Brain Res. 78:203-213.

Gainey MA, Feldman DE. 2017. Multiple shared mechanisms for homeostatic plasticity in rodent somatosensory and visual cortex. Philos Trans R Soc Lond B Biol Sci. 372.

Gamanut R, Kennedy H, Toroczkai Z, Ercsey-Ravasz M, Van Essen DC, Knoblauch K, Burkhalter A. 2018. The Mouse Cortical Connectome, Characterized by an Ultra-Dense Cortical Graph, Maintains Specificity by Distinct Connectivity Profiles. Neuron. 97:698-715 e610.

Gamanut R, Shimaoka D. 2022. Anatomical and functional connectomes underlying hierarchical visual processing in mouse visual system. Brain Struct Funct. 227:1297-1315.

Gao E, DeAngelis GC, Burkhalter A. 2010. Parallel Input Channels to Mouse Primary Visual Cortex. The Journal of Neuroscience. 30:5912-5926.

Gao M, Maynard KR, Chokshi V, Song L, Jacobs C, Wang H, Tran T, Martinowich K, Lee HK. 2014. Rebound potentiation of inhibition in juvenile visual cortex requires vision-induced BDNF expression. J Neurosci. 34:10770-10779.

Gilissen SR, Arckens L. 2021. Posterior parietal cortex contributions to cross-modal brain plasticity upon sensory loss. Curr Opin Neurobiol. 67:16-25.

Glickfeld LL, Histed MH, Maunsell JH. 2013. Mouse primary visual cortex is used to detect both orientation and contrast changes. J Neurosci. 33:19416-19422.

Glickfeld LL, Olsen SR. 2017. Higher-Order Areas of the Mouse Visual Cortex. Annual Review of Vision Science. 3:251-273.

Godement P, Saillour P, Imbert M. 1979. Thalamic afferents to the visual cortex in congenitally anophthalmic mice. Neurosci Lett. 13:271-278.

Goldreich D, Kanics IM. 2006. Performance of blind and sighted humans on a tactile grating detection task. Percept Psychophys. 68:1363-1371.

Gudi-Mindermann H, Rimmele JM, Nolte G, Bruns P, Engel AK, Roder B. 2018. Working memory training in congenitally blind individuals results in an integration of occipital cortex in functional networks. Behav Brain Res. 348:31-41.

Guimerà R, Nunes Amaral LA. 2005. Functional cartography of complex metabolic networks. Nature. 433:895-900.

Hanganu IL, Ben-Ari Y, Khazipov R. 2006. Retinal waves trigger spindle bursts in the neonatal rat visual cortex. J Neurosci. 26:6728-6736.

Harris JA, Mihalas S, Hirokawa KE, Whitesell JD, Choi H, Bernard A, Bohn P, Caldejon S, Casal L, Cho A, Feiner A, Feng D, Gaudreault N, Gerfen CR, Graddis N, Groblewski PA, Henry AM, Ho A, Howard R, Knox JE, Kuan L, Kuang X, Lecoq J, Lesnar P, Li Y, Luviano J, McConoughey S, Mortrud MT, Naeemi M, Ng L, Oh SW, Ouellette B, Shen E, Sorensen SA, Wakeman W, Wang Q, Wang Y, Williford A, Phillips JW, Jones AR, Koch C, Zeng H. 2019. Hierarchical organization of cortical and thalamic connectivity. Nature. 575:195-202.

Harris KD, Mrsic-Flogel TD. 2013. Cortical connectivity and sensory coding. Nature. 503:51-58.

Harris KD, Shepherd GMG. 2015. The neocortical circuit: themes and variations. Nature neuroscience. 18:170-181.

Hawellek DJ, Schepers IM, Roeder B, Engel AK, Siegel M, Hipp JF. 2013. Altered intrinsic neuronal interactions in the visual cortex of the blind. J Neurosci. 33:17072-17080.

Heimel JA, Hermans JM, Sommeijer JP, Neuro-Bsik Mouse Phenomics c, Levelt CN. 2008. Genetic control of experience-dependent plasticity in the visual cortex. Genes Brain Behav. 7:915-923.

Heine L, Bahri MA, Cavaliere C, Soddu A, Laureys S, Ptito M, Kupers R. 2015. Prevalence of increases in functional connectivity in visual, somatosensory and language areas in congenital blindness. Front Neuroanat. 9:86.

Hellyer PJ, Jachs B, Clopath C, Leech R. 2016. Local inhibitory plasticity tunes macroscopic brain dynamics and allows the emergence of functional brain networks. NeuroImage. 124:85-95.

Hensch TK. 2005. Critical period mechanisms in developing visual cortex. Curr Top Dev Biol. 69:215-237.

Hindley EL, Nelson AJ, Aggleton JP, Vann SD. 2014. Dysgranular retrosplenial cortex lesions in rats disrupt cross-modal object recognition. Learn Mem. 21:171-179.

Hou F, Liu X, Zhou Z, Zhou J, Li H. 2017. Reduction of Interhemispheric Functional Brain Connectivity in Early Blindness: A Resting-State fMRI Study. Biomed Res Int. 2017:6756927.

Hyvarinen J, Hyvarinen L, Linnankoski I. 1981. Modification of parietal association cortex and functional blindness after binocular deprivation in young monkeys. Exp Brain Res. 42:1-8.

Innocenti GM, Frost DO, Illes J. 1985. Maturation of visual callosal connections in visually deprived kittens: a challenging critical period. J Neurosci. 5:255-267.

Iurilli G, Ghezzi D, Olcese U, Lassi G, Nazzaro C, Tonini R, Tucci V, Benfenati F, Medini P. 2012. Sound-driven synaptic inhibition in primary visual cortex. Neuron. 73:814-828.

Jin L, Lange W, Kempmann A, Maybeck V, Gunther A, Gruteser N, Baumann A, Offenhausser A. 2016. High-efficiency transduction and specific expression of ChR2opt for optogenetic manipulation of primary cortical neurons mediated by recombinant adeno-associated viruses. J Biotechnol. 233:171-180.

Kanjlia S, Lane C, Feigenson L, Bedny M. 2016. Absence of visual experience modifies the neural basis of numerical thinking. Proceedings of the National Academy of Sciences. 113:11172-11177.

Kaschube M, Wolf F, Geisel T, Löwel S. 2002. Genetic Influence on Quantitative Features of Neocortical Architecture. The Journal of Neuroscience. 22:7206-7217.

Keck T, Keller GB, Jacobsen RI, Eysel UT, Bonhoeffer T, Hubener M. 2013. Synaptic scaling and homeostatic plasticity in the mouse visual cortex in vivo. Neuron. 80:327-334.

Klinge C, Eippert F, Roder B, Buchel C. 2010. Corticocortical connections mediate primary visual cortex responses to auditory stimulation in the blind. J Neurosci. 30:12798-12805.

Knyazev GG. 2007. Motivation, emotion, and their inhibitory control mirrored in brain oscillations. Neuroscience & Biobehavioral Reviews. 31:377-395.

Kraft AW, Mitra A, Bauer AQ, Snyder AZ, Raichle ME, Culver JP, Lee JM. 2017. Visual experience sculpts whole-cortex spontaneous infraslow activity patterns through an Arc-dependent mechanism. Proc Natl Acad Sci U S A. 114:E9952-E9961.

Kriegseis A, Hennighausen E, Rosler F, Roder B. 2006. Reduced EEG alpha activity over parieto-occipital brain areas in congenitally blind adults. Clin Neurophysiol. 117:1560-1573.

Kugler S, Kilic E, Bahr M. 2003. Human synapsin 1 gene promoter confers highly neuron-specific long-term transgene expression from an adenoviral vector in the adult rat brain depending on the transduced area. Gene Ther. 10:337-347.

Kujala T, Alho K, Huotilainen M, Ilmoniemi RJ, Lehtokoski A, Leinonen A, Rinne T, Salonen O, Sinkkonen J, Standertskjold-Nordenstam CG, Naatanen R. 1997. Electrophysiological evidence for cross-modal plasticity in humans with early- and late-onset blindness. Psychophysiology. 34:213-216.

Lambo ME, Turrigiano GG. 2013. Synaptic and Intrinsic Homeostatic Mechanisms Cooperate to Increase L2/3 Pyramidal Neuron Excitability during a Late Phase of Critical Period Plasticity. The Journal of Neuroscience. 33:8810.

Laramée ME, Bronchti G, Boire D. 2014. Primary visual cortex projections to extrastriate cortices in enucleated and anophthalmic mice. Brain Struct Funct. 219:2051-2070.

Laramée ME, Kurotani T, Rockland KS, Bronchti G, Boire D. 2011. Indirect pathway between the primary auditory and visual cortices through layer V pyramidal neurons in V2L in mouse and the effects of bilateral enucleation. Eur J Neurosci. 34:65-78.

Lepore N, Voss P, Lepore F, Chou YY, Fortin M, Gougoux F, Lee AD, Brun C, Lassonde M, Madsen SK, Toga AW, Thompson PM. 2010. Brain structure changes visualized in early- and late-onset blind subjects. Neuroimage. 49:134-140.

Lessard N, Paré M, Lepore F, Lassonde M. 1998. Early-blind human subjects localize sound sources better than sighted subjects. Nature. 395:278-280.

Liu Y, Yu C, Liang M, Li J, Tian L, Zhou Y, Qin W, Li K, Jiang T. 2007. Whole brain functional connectivity in the early blind. Brain. 130:2085-2096.

Lohmann G, Margulies DS, Horstmann A, Pleger B, Lepsien J, Goldhahn D, Schloegl H, Stumvoll M, Villringer A, Turner R. 2010. Eigenvector centrality mapping for analyzing connectivity patterns in fMRI data of the human brain. PLoS One. 5:e10232.

López-Bendito G, Aníbal-Martínez M, Martini FJ. 2022. Cross-Modal Plasticity in Brains Deprived of Visual Input Before Vision. Annu Rev Neurosci. 45:471-489.

Lubinus C, Orpella J, Keitel A, Gudi-Mindermann H, Engel AK, Roeder B, Rimmele JM. 2021. Data-Driven Classification of Spectral Profiles Reveals Brain Region-Specific Plasticity in Blindness. Cereb Cortex. 31:2505-2522.

Lund RD, Mitchell DE. 1979. The effects of dark-rearing on visual callosal connections of cats. Brain Res. 167:172-175.

Macaluso E. 2006. Multisensory Processing in Sensory-Specific Cortical Areas. The Neuroscientist. 12:327-338.

Macaluso E, Driver J. 2005. Multisensory spatial interactions: a window onto functional integration in the human brain. Trends in Neurosciences. 28:264-271.

Magrou L, Joyce MKP, Froudist-Walsh S, Datta D, Wang XJ, Martinez-Trujillo J, Arnsten AFT. 2024. The meso-connectomes of mouse, marmoset, and macaque: network organization and the emergence of higher cognition. Cereb Cortex. 34.

Massé IO, Guillemette S, Laramée ME, Bronchti G, Boire D. 2014. Strain differences of the effect of enucleation and anophthalmia on the size and growth of sensory cortices in mice. Brain Res. 1588:113-126.

Matsuzaki Y, Tanaka M, Hakoda S, Masuda T, Miyata R, Konno A, Hirai H. 2019. Neurotropic Properties of AAV-PHP.B Are Shared among Diverse Inbred Strains of Mice. Molecular Therapy. 27:700-704.

Meister M, Wong RO, Baylor DA, Shatz CJ. 1991. Synchronous bursts of action potentials in ganglion cells of the developing mammalian retina. Science. 252:939-943.

Meredith MA, Lomber SG. 2017. Species-dependent role of crossmodal connectivity among the primary sensory cortices. Hear Res. 343:83-91.

Michelson NJ, Vanni MP, Murphy TH. 2019. Comparison between transgenic and AAV-PHP.eB-mediated expression of GCaMP6s using in vivo wide-field functional imaging of brain activity. Neurophotonics. 6:025014.

Miller B, Chou L, Finlay BL. 1993. The early development of thalamocortical and corticothalamic projections. J Comp Neurol. 335:16-41.

Milleret C. 1994. Visual callosal connections and strabismus. Behav Brain Res. 64:85-95.

Missitzi J, Gentner R, Geladas N, Politis P, Karandreas N, Classen J, Klissouras V. 2011. Plasticity in human motor cortex is in part genetically determined. J Physiol. 589:297-306.

Mitra A, Snyder AZ, Hacker CD, Raichle ME. 2014. Lag structure in resting-state fMRI. J Neurophysiol. 111:2374-2391.

Mitra A, Snyder AZ, Tagliazucchi E, Laufs H, Raichle ME. 2015. Propagated infra-slow intrinsic brain activity reorganizes across wake and slow wave sleep. eLife. 4:e10781.

Mooney R, Penn AA, Gallego R, Shatz CJ. 1996. Thalamic relay of spontaneous retinal activity prior to vision. Neuron. 17:863-874.

Morimoto MM, Uchishiba E, Saleem AB. 2021. Organization of feedback projections to mouse primary visual cortex. iScience. 24:102450.

Murphy MC, Nau AC, Fisher C, Kim SG, Schuman JS, Chan KC. 2016. Top-down influence on the visual cortex of the blind during sensory substitution. Neuroimage. 125:932-940.

Noebels JL, Roth WT, Kopell BS. 1978. Cortical slow potentials and the occipital EEG in congenital blindness. J Neurol Sci. 37:51-58.

Noppeney U, Friston KJ, Ashburner J, Frackowiak R, Price CJ. 2005. Early visual deprivation induces structural plasticity in gray and white matter. Curr Biol. 15:R488-490.

Nunez PL. 2000. Toward a quantitative description of large-scale neocortical dynamic function and EEG. Behav Brain Sci. 23:371-398; discussion 399-437.

Oh SW, Harris JA, Ng L, Winslow B, Cain N, Mihalas S, Wang Q, Lau C, Kuan L, Henry AM, Mortrud MT, Ouellette B, Nguyen TN, Sorensen SA, Slaughterbeck CR, Wakeman W, Li Y, Feng D, Ho A, Nicholas E, Hirokawa KE, Bohn P, Joines KM, Peng H, Hawrylycz MJ, Phillips JW, Hohmann JG, Wohnoutka P, Gerfen CR, Koch C, Bernard A, Dang C, Jones AR, Zeng H. 2014. A mesoscale connectome of the mouse brain. Nature. 508:207-214.

Olavarria J, Bravo H, Ruiz G. 1988. The pattern of callosal connections in posterior neocortex of congenitally anophthalmic rats. Anat Embryol (Berl). 178:155-159.

Olavarria J, Malach R, Van Sluyters RC. 1987. Development of visual callosal connections in neonatally enucleated rats. J Comp Neurol. 260:321-348.

Olavarria J, van Sluyters RC. 1984. Callosal connections of the posterior neocortex in normal-eyed, congenitally anophthalmic, and neonatally enucleated mice. J Comp Neurol. 230:249-268.

Olavarria JF, Li CP. 1995. Effects of neonatal enucleation on the organization of callosal linkages in striate cortex of the rat. J Comp Neurol. 361:138-151.

Ortiz-Terán L, Diez I, Ortiz T, Perez DL, Aragón JI, Costumero V, Pascual-Leone A, El Fakhri G, Sepulcre J. 2017. Brain circuit-gene expression relationships and neuroplasticity of multisensory cortices in blind children. Proc Natl Acad Sci U S A. 114:6830-6835.

Oude Lohuis MN, Marchesi P, Olcese U, Pennartz CMA. 2024. Triple dissociation of visual, auditory and motor processing in mouse primary visual cortex. Nat Neurosci. 27:758-771.

Palva JM, Palva S. 2018. Functional integration across oscillation frequencies by cross-frequency phase synchronization. Eur J Neurosci. 48:2399-2406.

Petrus E, Isaiah A, Jones Adam P, Li D, Wang H, Lee H-K, Kanold Patrick O. 2014. Crossmodal Induction of Thalamocortical Potentiation Leads to Enhanced Information Processing in the Auditory Cortex. Neuron. 81:664-673.

Petrus E, Rodriguez G, Patterson R, Connor B, Kanold PO, Lee HK. 2015. Vision loss shifts the balance of feedforward and intracortical circuits in opposite directions in mouse primary auditory and visual cortices. J Neurosci. 35:8790-8801.

Piché M, Robert S, Miceli D, Bronchti G. 2004. Environmental enrichment enhances auditory takeover of the occipital cortex in anophthalmic mice. Eur J Neurosci. 20:3463-3472.

Poirier C, Collignon O, Scheiber C, Renier L, Vanlierde A, Tranduy D, Veraart C, De Volder AG. 2006. Auditory motion perception activates visual motion areas in early blind subjects. Neuroimage. 31:279-285.

Power JD, Cohen AL, Nelson SM, Wig GS, Barnes KA, Church JA, Vogel AC, Laumann TO, Miezin FM, Schlaggar BL, Petersen SE. 2011. Functional network organization of the human brain. Neuron. 72:665-678.

Ptito M, Matteau I, Zhi Wang A, Paulson OB, Siebner HR, Kupers R. 2012. Crossmodal recruitment of the ventral visual stream in congenital blindness. Neural Plast. 2012:304045.

Ptito M, Schneider FC, Paulson OB, Kupers R. 2008. Alterations of the visual pathways in congenital blindness. Exp Brain Res. 187:41-49.

Qin W, Liu Y, Jiang T, Yu C. 2013. The development of visual areas depends differently on visual experience. PLoS One. 8:e53784.

Renier L, Cuevas I, Grandin CB, Dricot L, Plaza P, Lerens E, Rombaux P, De Volder AG. 2013. Right Occipital Cortex Activation Correlates with Superior Odor Processing Performance in the Early Blind. PLOS ONE. 8:e71907.

Rhoades RW, Mooney RD, Fish SE. 1984. A comparison of visual callosal organization in normal, bilaterally enucleated and congenitally anophthalmic mice. Exp Brain Res. 56:92-105.

Rhoades RW, Mooney RD, Fish SE. 1985. Subcortical projections of area 17 in the anophthalmic mouse. Brain Res. 349:171-181.

Ricciardi E, Bonino D, Pellegrini S, Pietrini P. 2014. Mind the blind brain to understand the sighted one! Is there a supramodal cortical functional architecture? Neurosci Biobehav Rev. 41:64-77.

Ricciardi E, Tozzi L, Leo A, Pietrini P. 2014. Modality dependent cross-modal functional reorganization following congenital visual deprivation within occipital areas: a meta-analysis of tactile and auditory studies. Multisens Res. 27:247-262.

Rimmele JM, Gudi-Mindermann H, Nolte G, Röder B, Engel AK. 2019. Working memory training integrates visual cortex into beta-band networks in congenitally blind individuals. Neuroimage. 194:259-271.

Rocha RP, Koçillari L, Suweis S, Corbetta M, Maritan A. 2018. Homeostatic plasticity and emergence of functional networks in a whole-brain model at criticality. Scientific Reports. 8:15682.

Roder B, Rosler F, Hennighausen E, Nacker F. 1996. Event-related potentials during auditory and somatosensory discrimination in sighted and blind human subjects. Brain Res Cogn Brain Res. 4:77-93.

Roder B, Teder-Salejarvi W, Sterr A, Rosler F, Hillyard SA, Neville HJ. 1999. Improved auditory spatial tuning in blind humans. Nature. 400:162-166.

Rubinov M, Sporns O. 2010. Complex network measures of brain connectivity: uses and interpretations. Neuroimage. 52:1059-1069.

Saccone EJ, Tian M, Bedny M. 2024. Developing cortex is functionally pluripotent: Evidence from blindness. Dev Cogn Neurosci. 66:101360.

Sadato N, Pascual-Leone A, Grafman J, Deiber MP, Ibanez V, Hallett M. 1998. Neural networks for Braille reading by the blind. Brain. 121 (Pt 7):1213-1229.

Sadato N, Pascual-Leone A, Grafman J, Ibañez V, Deiber M-P, Dold G, Hallett M. 1996. Activation of the primary visual cortex by Braille reading in blind subjects. Nature. 380:526-528.

Saleem AB. 2020. Two stream hypothesis of visual processing for navigation in mouse. Curr Opin Neurobiol. 64:70-78.

Schepers IM, Hipp JF, Schneider TR, Roder B, Engel AK. 2012. Functionally specific oscillatory activity correlates between visual and auditory cortex in the blind. Brain. 135:922-934.

Schmidt R, LaFleur KJ, de Reus MA, van den Berg LH, van den Heuvel MP. 2015. Kuramoto model simulation of neural hubs and dynamic synchrony in the human cerebral connectome. BMC Neurosci. 16:54.

Schubert JT, Buchholz VN, Focker J, Engel AK, Roder B, Heed T. 2015. Oscillatory activity reflects differential use of spatial reference frames by sighted and blind individuals in tactile attention. Neuroimage. 117:417-428.

Sforazzini F, Schwarz AJ, Galbusera A, Bifone A, Gozzi A. 2014. Distributed BOLD and CBV-weighted resting-state networks in the mouse brain. Neuroimage. 87:403-415.

Shimony J, Burton H, Adrian AE, McLaren D, Shu-wei S, Snyder A. 2006. Diffusion tensor imaging reveals white matter reorganization in early blind humans. Cerebral Cortex. 16:1653-1661.

Shu N, Liu Y, Li J, Li Y, Yu C, Jiang T. 2009. Altered anatomical network in early blindness revealed by diffusion tensor tractography. PLoS One. 4:e7228.

Smolders K, Vreysen S, Laramée M-E, Cuyvers A, Hu T-T, Van Brussel L, Eysel UT, Nys J, Arckens L. 2016. Retinal lesions induce fast intrinsic cortical plasticity in adult mouse visual system. European Journal of Neuroscience. 44:2165-2175.

Striem-Amit E, Ovadia-Caro S, Caramazza A, Margulies DS, Villringer A, Amedi A. 2015. Functional connectivity of visual cortex in the blind follows retinotopic organization principles. Brain. 138:1679-1695.

Tian M, Xiao X, Hu H, Cusack R, Bedny M. 2023. Visual experience shapes functional connectivity between occipital and non-visual networks. bioRxiv.

Tomaiuolo F, Campana S, Collins DL, Fonov VS, Ricciardi E, Sartori G, Pietrini P, Kupers R, Ptito M. 2014. Morphometric Changes of the Corpus Callosum in Congenital Blindness. PLOS ONE. 9:e107871.

Touj S, Tokunaga R, Al Aïn S, Bronchti G, Piché M. 2019. Pain Hypersensitivity is Associated with Increased Amygdala Volume and c-Fos Immunoreactivity in Anophthalmic Mice. Neuroscience. 418:37-49.

Tucker P, Laemle L, Munson A, Kanekar S, Oliver ER, Brown N, Schlecht H, Vetter M, Glaser T. 2001. The eyeless mouse mutation (ey1) removes an alternative start codon from the Rx/rax homeobox gene. Genesis. 31:43-53.

Turley JA, Zalewska K, Nilsson M, Walker FR, Johnson SJ. 2017. An analysis of signal processing algorithm performance for cortical intrinsic optical signal imaging and strategies for algorithm selection. Scientific Reports. 7:7198.

Uhlhaas PJ, Haenschel C, Nikolić D, Singer W. 2008. The role of oscillations and synchrony in cortical networks and their putative relevance for the pathophysiology of schizophrenia. Schizophr Bull. 34:927-943.

Valley MT, Moore MG, Zhuang J, Mesa N, Castelli D, Sullivan D, Reimers M, Waters J. 2020. Separation of hemodynamic signals from GCaMP fluorescence measured with wide-field imaging. Journal of Neurophysiology. 123:356-366.

van den Heuvel MP, Sporns O. 2011. Rich-club organization of the human connectome. J Neurosci. 31:15775-15786.

van der Heijden K, Formisano E, Valente G, Zhan M, Kupers R, de Gelder B. 2019. Reorganization of Sound Location Processing in the Auditory Cortex of Blind Humans. Cerebral Cortex. 30:1103-1116.

Vanhatalo S, Palva JM, Holmes MD, Miller JW, Voipio J, Kaila K. 2004. Infraslow oscillations modulate excitability and interictal epileptic activity in the human cortex during sleep. Proc Natl Acad Sci U S A. 101:5053-5057.

Wang D, Qin W, Liu Y, Zhang Y, Jiang T, Yu C. 2014. Altered resting-state network connectivity in congenital blind. Hum Brain Mapp. 35:2573-2581.

Wang Q, Sporns O, Burkhalter A. 2012. Network Analysis of Corticocortical Connections Reveals Ventral and Dorsal Processing Streams in Mouse Visual Cortex. The Journal of Neuroscience. 32:4386-4399.

Watkins KE, Cowey A, Alexander I, Filippini N, Kennedy JM, Smith SM, Ragge N, Bridge H. 2012. Language networks in anophthalmia: maintained hierarchy of processing in 'visual' cortex. Brain. 135:1566-1577.

Weeks R, Horwitz B, Aziz-Sultan A, Tian B, Wessinger CM, Cohen LG, Hallett M, Rauschecker JP. 2000. A positron emission tomographic study of auditory localization in the congenitally blind. J Neurosci. 20:2664-2672.

Weliky M, Katz LC. 1999. Correlational structure of spontaneous neuronal activity in the developing lateral geniculate nucleus in vivo. Science. 285:599-604.

Wittenberg G, Werhahn K, Wassermann E, Herscovitch P, Cohen L. 2004. Functional connectivity between somatosensory and visual cortex in ear ly blind humans. European Journal of Neuroscience.

Wong RO, Meister M, Shatz CJ. 1993. Transient period of correlated bursting activity during development of the mammalian retina. Neuron. 11:923-938.

Yu C, Liu Y, Li J, Zhou Y, Wang K, Tian L, Qin W, Jiang T, Li K. 2008. Altered functional connectivity of primary visual cortex in early blindness. Hum Brain Mapp. 29:533-543.

Zingg B, Hintiryan H, Gou L, Song MY, Bay M, Bienkowski MS, Foster NN, Yamashita S, Bowman I, Toga AW, Dong H-W. 2014. Neural networks of the mouse neocortex. Cell. 156:1096-1111.

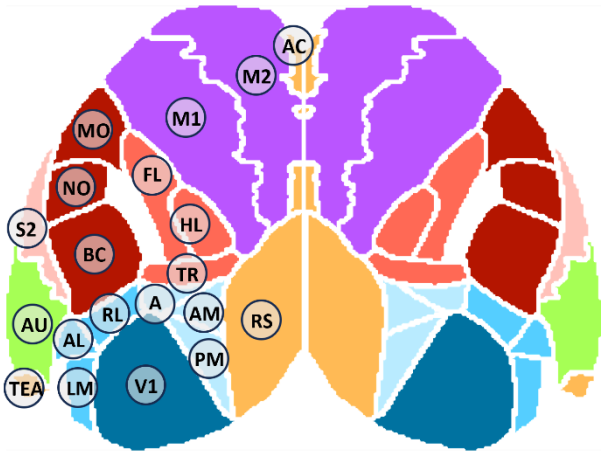

Figure 1 – Schematic Representation of the Dorsal Cortical Areas Mask

Schematic representation of the mask used for the parcellation of the dorsal cortical areas of the mouse brain, based on the CCF Allen Brain Atlas. Associative areas (AC, RS and TEA) are yellow. Motor areas (M1 and M2) are in purple, and somatosensory areas in shades of red. Trigeminal-related sensory regions (MO, NO, and BC) are in dark red, while dorsal column-related regions (FL, HL, and TR) are shown in salmon, with S2 in pink. Visual areas are in shades of blue: V1 in dark blue, lateral visual areas (AL, LM, and RL) in ocean blue, and medial visual areas (A, AM, and PM) in meltwater blue. Auditory area (AU) is represented in green.

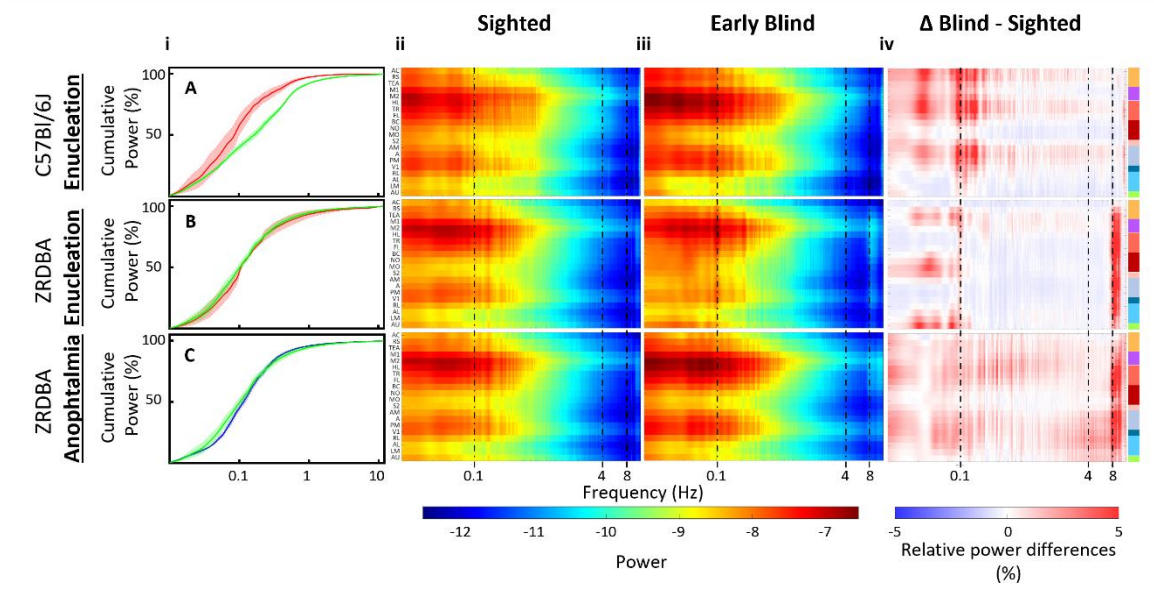

Figure 2 – Resting state Cortical power Spectral Signatures in Sighted and Blind C57Bl6J and ZRDBA Mice

Influence of the perinatal enucleation on C57Bl/6J mice (**A**), on ZRDBA mice (**B**) and anophtalmia on ZRDBA mice (**C**).

(**i**) Relative cumulative power across oscillation frequencies (0.0125–12 Hz) during resting-state acquisition; curves represent group means (solid lines) with SEM (dotted lines).

(**ii**) Smoothed $\log_{10}$ spectral power in sighted control mice across 20 cortical ROIs on a logarithmic frequency axis.

(**iii**) Corresponding spectral power profiles in early visually deprived mice.

(**iv**) Relative power difference maps (Blind – Sighted), highlighting increases (red) or decreases (blue) in power for each ROI. Dashed vertical lines indicate canonical frequency bands: infraslow (<0.1 Hz), delta (0.1–4 Hz), theta (4–8 Hz), and mu (8–12 Hz).

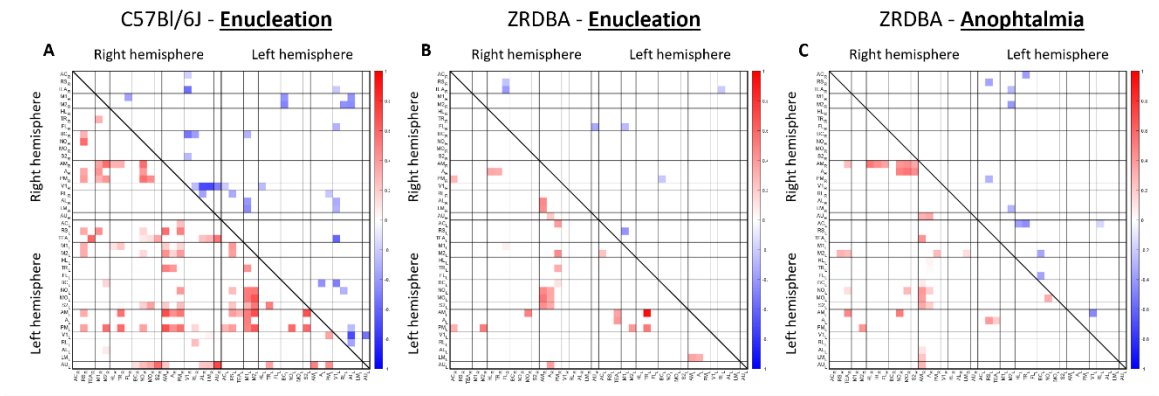

Figure 3 - Altered functional connectivity following early visual deprivation.

Significant inter-regional correlation differences (Welch's t-test, $p < 0.05$, uncorrected) between early visually deprived mice and sighted controls. Positive differences appear in the lower triangle, negative differences in the upper triangle. (A) C57Bl/6J mice sighted vs. enucleated, (B) ZRDBA mice sighted vs. enucleated and (C) ZRDBA mice sighted vs. anophthalmic. Regions are organized by hemisphere (right and left) and functional domains (associative, motor, somatosensory, visual and auditory).

Following enucleation in the C57 mice there was a more evident trend for increased than decreased temporal resting state correlations both within and between hemispheres. Increases in ipsilateral functional connectivity was mainly evident between medial HVA (AM, A, PM) and motor cortices (M1 and M2) and with somatosensory areas (MO, NO S2). Increases in interhemispheric connectivity were evident between medial HVAs (homotopic AM and PM) and between these HVAs and motor areas M1 and M2. Increased interhemispheric connectivity was also significant between homotopic auditory cortices and between auditory cortex and lateral HVAs AL and LM and with somatosensory areas BC, No, MO and S2. Intrahemispheric disconnections were most notable between the primary visual cortex and lateral HVAs (RL, AL, LM). The trend for increased functional

connectivity was not as apparent following enucleation and anophthalmia in the ZRDBA mice. The strongest increased connectivity was observed both ipsilaterally and contralaterally between medial HVAs (AM, A) and the somatosensory areas NO, MO and S2 in enucleated as well as in anophthalmic ZRDBA mice.

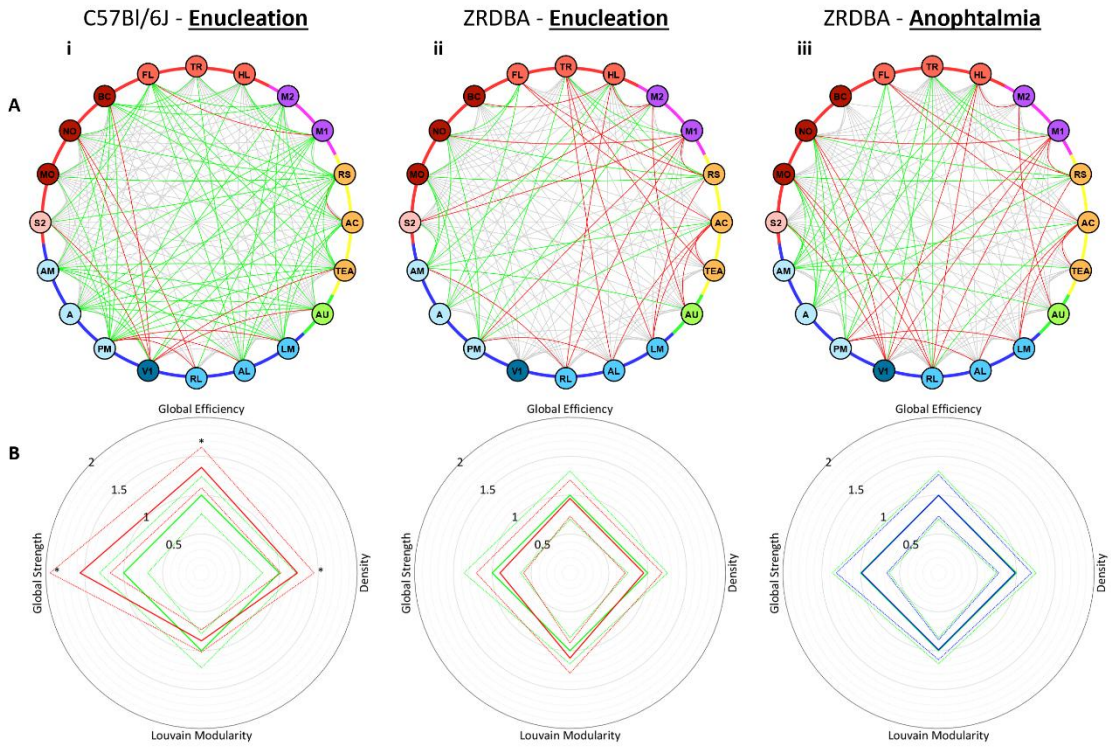

Figure 4 – Differential Circular Connectome Diagram and Global Network Metrics

Influence of the perinatal enucleation on C57Bl/6J mice (**i**), on ZRDBA mice (**ii**) and anophtalmia on ZRDBA mice (**iii**).

A. The circular connectome diagram of the connectivity patterns between cortical regions (nodes), Suprathreshold z-score (>0.3) connectivity between nodes is depicted with colored edges. Grey links represent connectivity present in both sighted and blind mice, green links indicate suprathreshold connections unique to the blind mice, and red links show connections lost in the blind mice. Perimeter colors represent functional modules as described in Figure 1 (Associative areas (AC, RS and TEA) are yellow. Motor areas (M1 and M2) are in purple, and somatosensory areas in shades of red. Trigeminal sensory regions (MO, NO, and BC) are in dark red, while dorsal column-related regions (FL, HL,

and TR) are shown in salmon, with S2 in pink. Auditory area (AU) is represented in green. Visual areas are in shades of blue: V1 in dark blue, lateral visual areas (AL, LM, and RL) in ocean blue, and medial visual areas (A, AM, and PM) in meltwater blue).

B. Comparison of global network metrics: Four global network metrics—global efficiency (North), network density (East), Louvain modularity (South), and global strength (West)—are compared between sighted (green) and blind groups (red: enucleated, blue: anophthalmic). Metrics are normalized to the mean values of the sighted group (centered at 1). Darker lines represent group means, and lighter lines indicate SEM. Statistically significant differences ($p \leq 0.05$, Bonferroni-corrected pairwise tests) are denoted by asterisks (*).

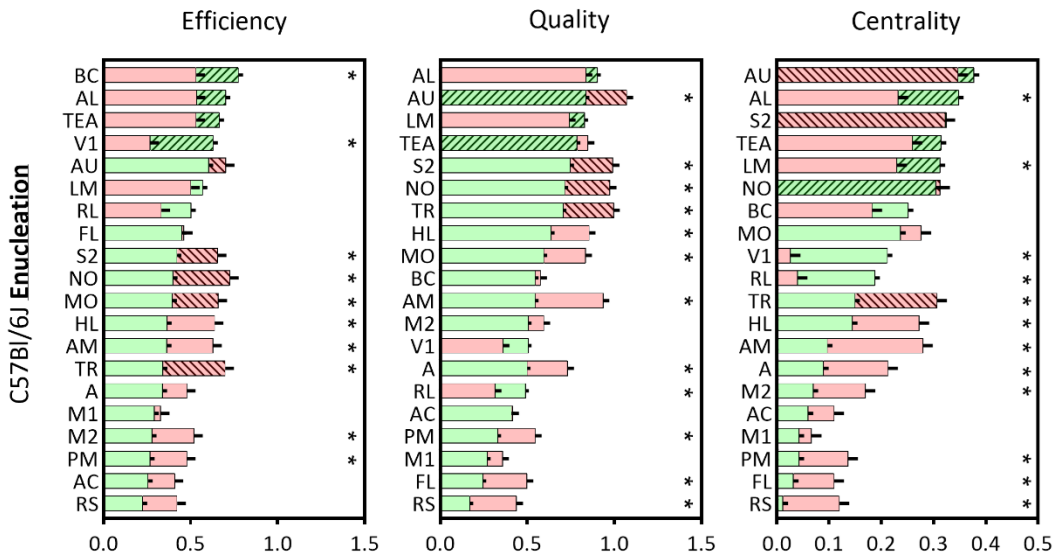

Figure 5 – Effects of Early Visual Deprivation on Cortical Nodal Influence Metrics in C57Bl/6J Mice

Cortical distributions of nodal influence metrics—including efficiency, connectivity strength, and eigenvector centrality—are shown for sighted (green) and enucleated (red) C57Bl/6J mice. Cortical areas are ranked from the highest to the lowest values based on the sighted group (top to bottom). Hatched bars indicate cortical hubs for each metric, defined as nodes with values exceeding 1 standard deviation above the network mean. Error bars represent the standard error of the mean (SEM). Statistically significant differences between sighted and enucleated groups are indicated by asterisks (*), corresponding to Bonferroni corrected p-values ≤ 0.05.

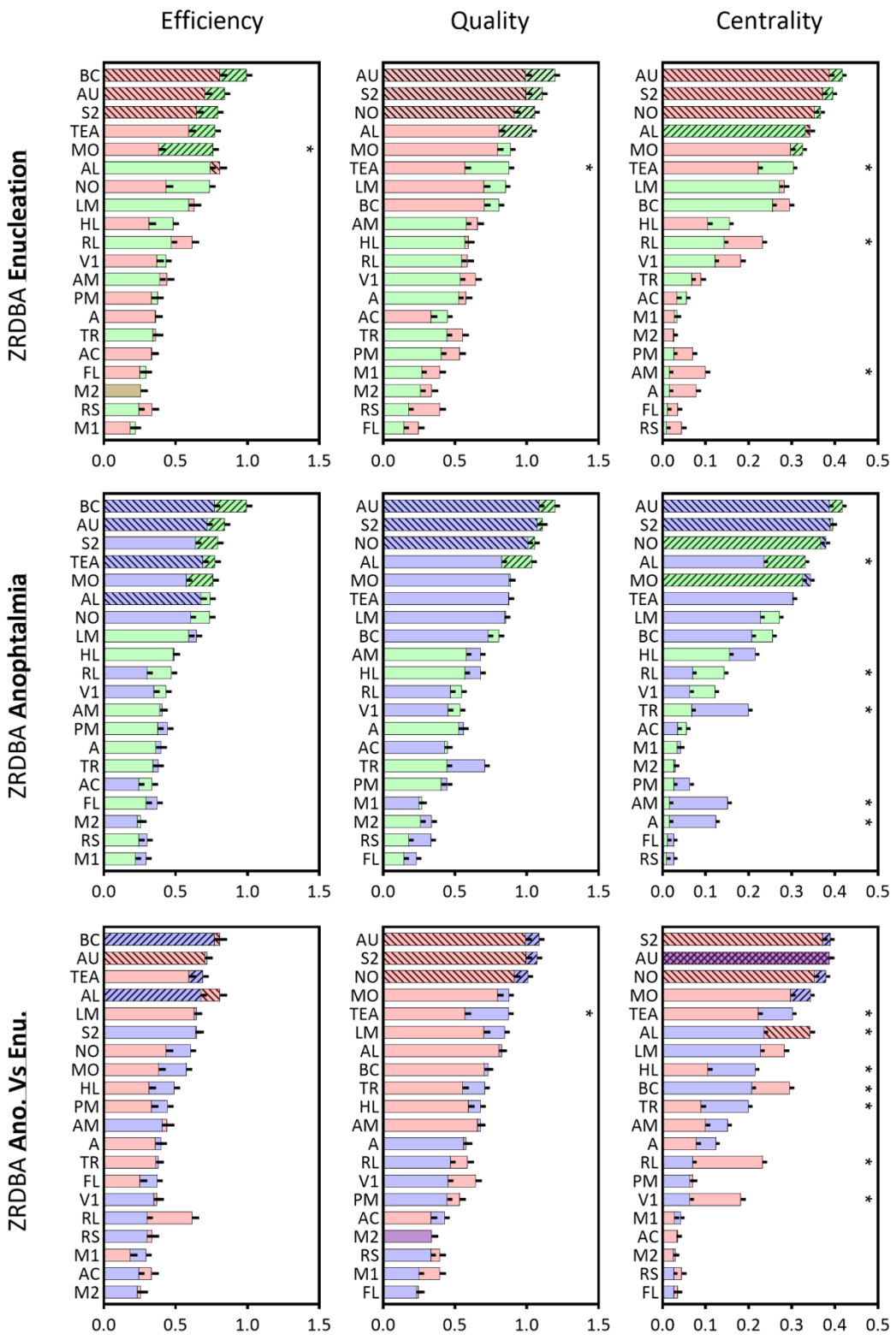
Efficiency
Quality
Centrality
ZRDBA Enucleation
ZRDBA Anophtalmia
ZRDBA Ano._Vs_Enu.
BC AU S2 TEA MO AL NO LM HL RL V1 AM PM A TR AC FL M2 RS M1
AU S2 NO AL MO TEA LM BC AM HL RL V1 A AC TR PM M1 M2 RS FL
AU S2 NO AL MO TEA LM BC HL RL V1 TR AC M1 M2 PM AM A FL RS
0.0 0.5 1.0 1.5
0.0 0.1 0.2 0.3 0.4 0.5

Figure 6 – Effects of Early Visual Deprivation on Cortical Nodal Influence Metrics in ZRDBA Mice

Cortical distributions of nodal influence metrics—including efficiency, connectivity strength, and eigenvector centrality—are shown for sighted (green), enucleated (red) and anophtalmic (blue) ZRDBA mice. Cortical areas are ranked from the highest to the lowest values based on the sighted group (top to bottom). Hatched bars indicate cortical hubs for each metric, defined as nodes with values exceeding 1 standard deviation above the network mean. Error bars represent the standard error of the mean (SEM). Statistically significant differences between sighted and enucleated groups are indicated by asterisks (*), corresponding to Bonferroni corrected p-values ≤ 0.05.

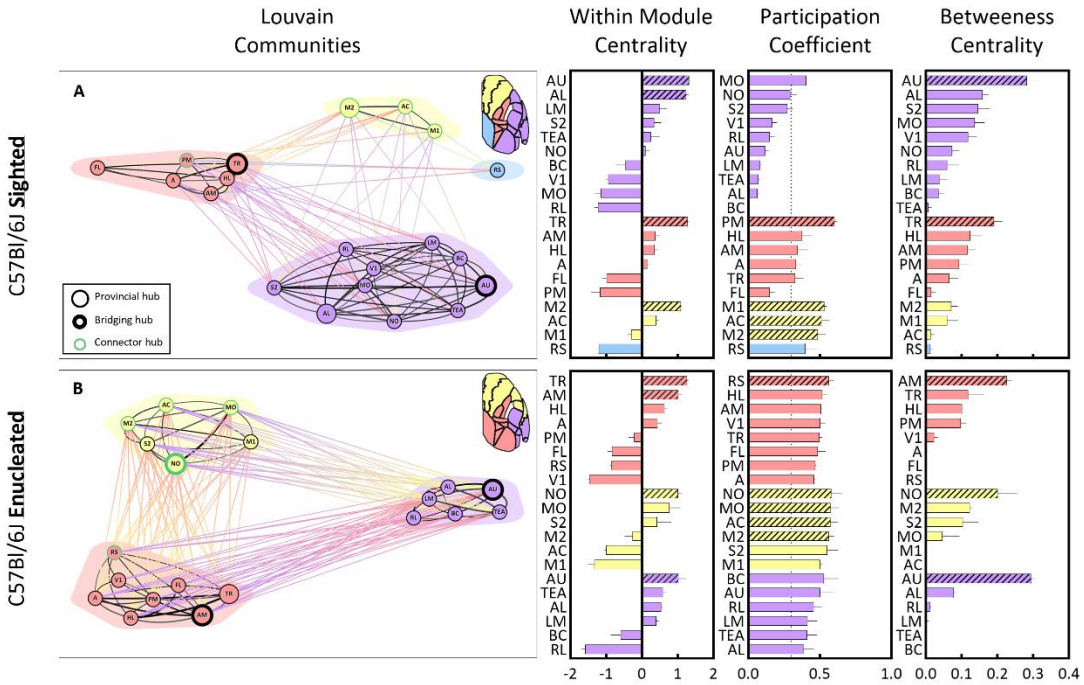

Figure 7 – Network Community Structure in sighted (A) and enucleated (B) C57Bl/6J mice

Schematic representation of the impact of early visual deprivation by enucleation on the consensus community structure in C57Bl/6J mice. Community affiliations, identified using Louvain modularity analysis, are color-coded throughout the figure. Provincial hubs are represented by larger-sized markers, connector nodes are outlined with green borders, and bridging nodes feature thicker marker outlines. Connection thickness is weighted based on the strength of correlation. Intra-modular connections are depicted in shades of black, while inter-modular connections are color-coded according to the respective modules they connect. Structural nodal metrics of the right hemisphere network—including within-module degree centrality, participation coefficient, and betweenness centrality—are presented for cortical areas, ranked within each community from highest to lowest based

on values from the sighted group. Hatched bars indicate cortical hubs, defined as nodes with metric values exceeding one standard deviation above the network mean. Error bars represent the standard error of the mean (SEM).

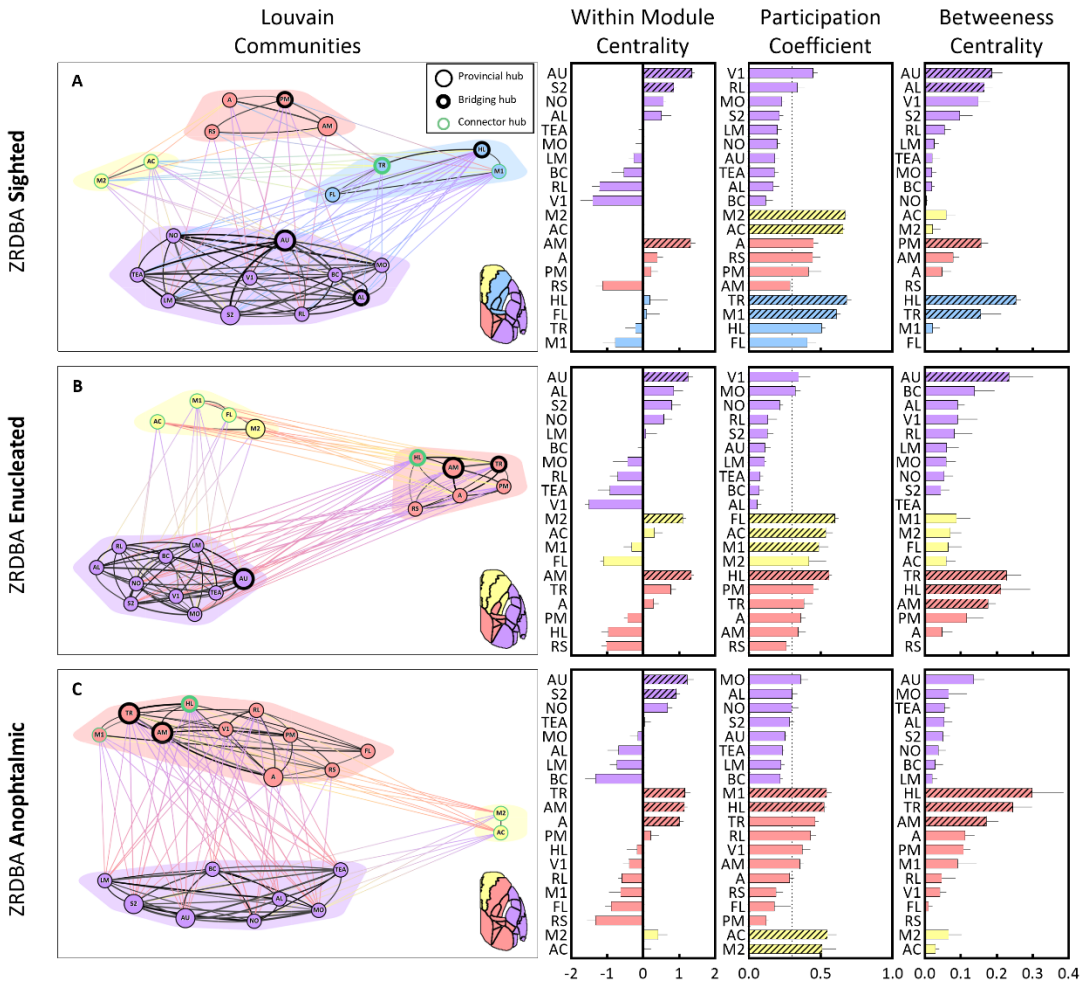

Figure 8 – Network Community Structure in sighted (A), enucleated (B) and anophtalmic (C) ZRDBA mice

Schematic representation of the impact of early visual deprivation by enucleation and anophtalmia on the consensus community structure in ZRDBA mice. Community affiliations, identified using Louvain modularity analysis, are color-coded throughout the figure. Provincial hubs are represented by larger-sized markers, connector nodes are outlined with green borders, and bridging nodes feature thicker marker outlines. Connection thickness is weighted based on the strength of correlation. Intra-modular

connections are depicted in shades of black, while inter-modular connections are color-coded according to the respective modules they connect. Structural nodal metrics of the right hemisphere network—including within-module degree centrality, participation coefficient, and betweenness centrality—are presented for cortical areas, ranked within each community from highest to lowest based on values from the sighted group. Hatched bars indicate cortical hubs, defined as nodes with metric values exceeding one standard deviation above the network mean. Error bars represent the standard error of the mean (SEM).